A new open-source finite element lumbar spine model, its tuning and validation, and development of a tissue-based injury risk function for compression fractures

Johan Iraeus, Yash Niranjan Poojary, Leila Jaber, Jobin John, Johan Davidsson

Abstract Lumbar spine fractures have been identified as a problem in motor vehicle crashes, and it is expected that this problem might increase with the introduction of reclined postures in autonomous vehicles. Human body models provide a means to address this issue and develop countermeasures. In this study a new open-source finite element lumbar spine model and an associated tissue-based injury risk function were developed and validated. The injury risk function was based on trabecular bone compressive strain in the superior-inferior direction.

The kinematic and kinetic validation showed that the model compared reasonably to experimental data, with axial compression and flexion predictions being closest to experimental results. The new risk function was found to have a good quality index.

Even though the model evaluations indicated that the fracture risk was somewhat overpredicted, it was judged that the current model, together with the associated injury risk function, can be used to estimate the risk for compressive fractures in the lumbar spine, with the knowledge that these estimates are most likely somewhat conservative.

Keywords Lumbar spine, human body model, compression fracture, injury criteria, injury risk function.

I. INTRODUCTION

Epidemiology studies have identified lumbar spine fractures to be a problem in motor vehicle collisions [1-7]. While these injuries are overrepresented in crash types that include a vertical crash pulse component, they are also frequent in frontal and multiple impacts without a vertical component [2,3,6,7]. It has also been shown that the incidence has increased for newer vehicles [2,4,5,7]. Many studies have identified vertebrae compression and wedge fractures at levels T12-L1, resulting from axial compression and flexion, as the most frequent injury type and location [2,4,6]. These findings have also been confirmed in frontal crash tests using belted Post Mortem Human Subjects (PMHSs) [8-12]. With the introduction of autonomous vehicles, it is expected that vehicle passengers will ride in more reclined positions than is common today. This could increase the risk of lumbar spine fractures in frontal and multiple crashes if not properly addressed [11-16]. For this we need a validated tool with an associated injury risk function.

Finite Element (FE) Human Body Models (HBMs) have been shown to be a good complement to traditional crash test dummies, as they can predict omnidirectional kinematics and kinetics and offer the possibility to evaluate injury at tissue level. For FE models the tissue level is approximated by the results in the finite elements, so this level can also be referred to as element level and depending on the discretization this can correspond to different structural levels. Examples of some contemporary FE-HBMs for occupant safety are the Total Human Model for Safety (THUMS) [17], the Global Human Body Model Consortium (GHBMC) model [18], the SAFER HBM [19] and the VIVA+ HBM [20]. While both the THUMS (version 4+) and the detailed GHBMC models include detailed lumbar spine models, validation presented in the open literature is lacking. An exception is the evaluation of the detailed GHBMC lumbar spine model in axial compression and flexion presented in [21], where the authors concluded that the model lacked somewhat in biofidelity. The SAFER HBM as well as the VIVA+ models have simplified lumbar spines, partly modelled as rigid structures, not suitable for tissue-based injury evaluation.

Lumbar spine injury risks are currently estimated based on cross-sectional forces and moments, using Injury Risk Functions (IRFs) developed from biomechanical testing [22]. While this can work sufficiently when an

J. Iraeus (e-mail: johan.iraeus@chalmers.se) and J. John are Researchers, Y. N. Poojary and L. Jaber are Research Assistants, and J. Davidsson is an Associate Professor at the Department of Mechanics and Maritime Sciences at Chalmers University of Technology, Gothenburg, Sweden.

average-sized HBM is used, it is insufficient for morphed HBMs because most IRFs normally do not include size-dependent covariates. A more attractive way of evaluating lumbar spine injury risks using HBMs is to use a tissue based IRF (for example, stress or strain), which automatically scales with spine dimensions. None of the four HBMs presented above has an associated tissue based IRF for prediction of lumbar spine fracture risk.

Thus, the aim of this study was to develop and validate a lumbar spine FE model, targeted for inclusion in HBMs and for use in the design of vehicle restraints, and to generate an associated tissue-level IRF for endplate and vertebrae fractures. To make the model and associated IRF available to everyone, the model will be licensed as open source.

II. METHODS

A FE lumbar spine model, for inclusion in full HBMs, modelled with a mesh to enable tissue-based injury criteria of the vertebrae body, was created based on literature data. Specifically, the ligament unstretched length and the nucleus pulposus material properties were tuned based on Functional Spine Unit (FSU) data. Next, the kinetics and kinematics of the lumbar spine model were validated using published biomechanical data. Finally, a tissue based IRF targeting compression fractures in the spinal column was developed and evaluated. All simulations were carried out using LS-DYNA MPP R12.1.0 (ANSYS/LST, Livermore, CA). Meshing and other pre-processing were done using ANSA (Beta CAE Systems, Luzern, Switzerland), post-processing using LS-PREPOST (ANSYS/LST, Livermore, CA) and Hypergraph (Altair, Troy, MI), and development of the IRFs were carried out in R [23].

Development of a lumbar spine model

A lumbar spine FE mesh, with mesh quality criteria according to [19], was created using a hexa block design, see Fig. 1 for an example of the L4-L5 FSU, with nodal connectivity between the vertebrae body and the discs. The geometry was based on an average-sized female [24]. The element size was chosen based on a target time step of 0.5 µs in explicit FE solvers. The trabecular bone was modelled using reduced order hexahedral elements, while the cortical bone and endplates were modelled using fully integrated quad shell elements.

The trabecular bone material (main interest for capturing compression fractures in this study) was assumed to homogenous throughout the vertebrae body and modelled using an orthotropic material, see TABLE I for details.

TABLE I
MATERIAL MODELS AND PARAMETERS FOR THE LUMBAR SPINE MODEL

Material	LS-Dyna material model	Model parameters [mm, ms, GPa]	References
Trabecular vertebrae body	**MAT_ORTHOTROPIC_ELASTIC*	E_A=0.492, E_B=0.207, E_C=0.141, G_{AB}=0.064, G_{BC}=0.075, G_{CA}=0.09, v_{BA}=0.097, v_{CA}=0.115, v_{CB}=0.259	[25] [26]
Trabecular posterior	**MAT_PIECEWISE_LINEAR_PLASTICITY*	E=0.492, v=0.1	[25]
Cortical bone vertebrae body	**MAT_ANISTROPIC_ELASTIC_PLASTIC*	C_{11}=19.9, C_{12}=7.5, C_{13}=7.5, $C2_2$=17.0, C23=7.75, C_{33}=17.0, C_{44}=3.5, C_{55}=4.0, C_{66}=3.5, S_{11}=0.112, S_{22}=0.053, S_{33}=0.053, S_{12}=0.047	[27]
Cortical bone posterior	**MAT_PIECEWISE_LINEAR_PLASTICITY*	E=16.4, v=0.235, σ_Y=0.112, E_{tan}=0.924	[27]
Endplate	**MAT_PIECEWISE_LINEAR_PLASTICITY*	E=0.193, v=0.3, σ_Y=0.0037	[28]
Annulus fibers inner	**MAT_FABRIC*	E_A=0.0038, E_B=0.0038, v_{BA}=0.3, G_{AB}=0.0015, Beta=±45°	[29] [30]
Annulus fibers outer	**MAT_FABRIC*	E_A=0.0070, E_B=0.0070, v_{BA}=0.3, G_{AB}=0.0027, Beta=±64°	[29] [30]
Annuls ground	**MAT_HILL_FOAM*	K=2, N=2, MU=0.05, C_1=-0.000895, C_2=0.002101, C_3=0.000115, B_1=-2, B_2=-1, B_3=4	[31]
Nucleus Pulposus	**MAT_OGDEN_RUBBER*	v=0.49995, μ_1=0.000234, μ_2=-0.061, μ_3=0.086, α_1=15.69, α_1=3.07, α_1=2.2	
Ligaments	**MAT_ELASTIC_SPRING_DISCRETE_BEAM*		[32] [33] [34]

The trabecular bone in the posterior part of the vertebrae, of less importance for the compression fractures, was modelled using an isotropic material model. The inferior-superior direction was chosen as main direction

based on [25,35]. The anterior-posterior direction was chosen as second (strongest) direction and the lateral direction as the third based on biomechanical principles (muscle and ligament attachments and load paths).

The thicknesses (range 0.51–0.82 mm) of the cortical shells and endplates of the vertebrae bodies were defined according to [36], and then interpolated between reported sites. The cortical bone was modelled using an anisotropic material model, assuming a transversely isotropic material (assumed superior-inferior to be main direction). Similar to the trabecular bone, the cortical bone in the posterior part was modelled using an isotropic material model. The endplates were also modelled using an isotropic material model. More details on all materials can be found in TABLE I or in the openly available model.

The intervertebral discs were modelled using a combination of reduced order solid and fully integrated membrane elements. The annulus fibrosis was modelled using three layers of membrane elements (see Fig. 1). In reality the annulus fibrosis consists of many fibre layers with different angled fibres, but the minimum element size was restricted by the target time step, resulting in three fibre layers. The fibre directions of each layer (outer ± 64°, middle ± 54° and inner ± 45°) were assigned according to [29] and the membrane thicknesses according to [37]. The annulus fibres were modelled using a tensile only material model for fabrics, see TABLE I for more details. The annulus ground substance and nucleus pulposus were modelled using solid elements. The dimension of the nucleus was defined to be about 40% of the total disc area according to [38]. The annulus ground substance was modelled using a foam material model, while the nucleus pulposus was modelled using a rubber material model with material constants tuned to fit the average response in FSU compression tests (see next section). The Anterior Longitudinal (ALL), Posterior Longitudinal (PLL), Flavum (LF), Intertransverse (ITL) and Interspinous + Supraspinous (ISL+SSL) ligaments were modelled using non-linear elastic beam elements with force-deflection properties according to [32] and strain rate properties according to [33]. The Facet Capsular (FC) ligament instead used force-deflection properties according to [34].

No element erosion was implemented for any of the tissues modelled. An automatic single surface contact, with friction coefficient of 0.1, was defined, including all shells and membrane elements in the lumbar spine.

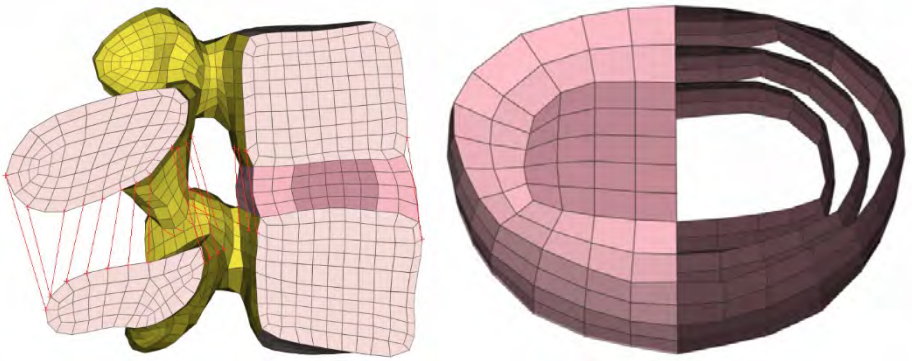

Fig. 1. Left: example mesh for the L4-L5 FSU. Right: modelling of intervertebral disc (the annulus ground substance and nucleus pulposus are removed from half of the disc in the figure for visualisation.

Tuning of nucleus properties and ligament initial length

The Ogden material parameters for the nucleus pulposus were manually tuned to fit FSU compression [39-42] and tension [40] responses. To capture the non-linear force-deflection behaviour seen in the tests, three Ogden terms were used. No viscos terms were included, meaning that strain rate effects were not modelled.

As the data sources for ligament mechanical properties [32,34] do not report the initial unstretched length corresponding to a neutral spine posture, this unstretched length had to be reverse-engineered (tuned) from lumbar spine FSU tests. This was done by simulating the stepwise reduction L4-L5 FSU tests reported in [43,44] (see Fig. 2). First, a model without any ligaments, and the nucleus pulposus removed, was simulated (step 1 in Fig. 2). Then ligaments or other anatomical structures were added one at a time and new simulations were run. This was carried out all the way to the intact FSU (step 9 in Fig. 2). At each step, the added ligament initial unstretched length was tuned to match the moment-rotation curves from the physical tests. The tuning was done by translating the ligament force-deflection curve along the abscissa, introducing either ligament pre-stretch or slack. For each step, flexion, extension, lateral bending as well as axial rotation were simulated and compared to the physical tests. As the two data sets used L4-L5 FSUs from both male and female donors, the L4-L5 FSU FE model (matching an average female in size) was scaled based on the averaged measurements of lumbar spine

vertebrae body dimensions in [45-48], presented in Appendix A. The vertebrae height was scaled by 1.02 while the anterior-posterior and transverse diameters were scaled by 1.11 to create average sized male vertebrates from the base (average sized female) model. Both the male and the female vertebrae sizes were simulated and compared to the results in [43,44]. In addition, to estimate the population effect, the average covariation 7.9% (SD/average) [45-48], was used to create a small female vertebra (1 SD below the average female) and a large male vertebrae (1 SD above the average male). These two additional sizes were included in the comparison to the results for the intact vertebrae. Finally, a parameter "LUMB_FLEX" was introduced. This parameter scales the ligament pre-stretch/slack depending on the spine initial curvature. Recommended values are -1 for a lordotic (neutral) spine, which is typical for a standing person, and 0 for a straight (flexed) spine, which is typical for a seated vehicle occupant. It was assumed that the same scaling could be used for ligaments at all levels of the lumbar spine.

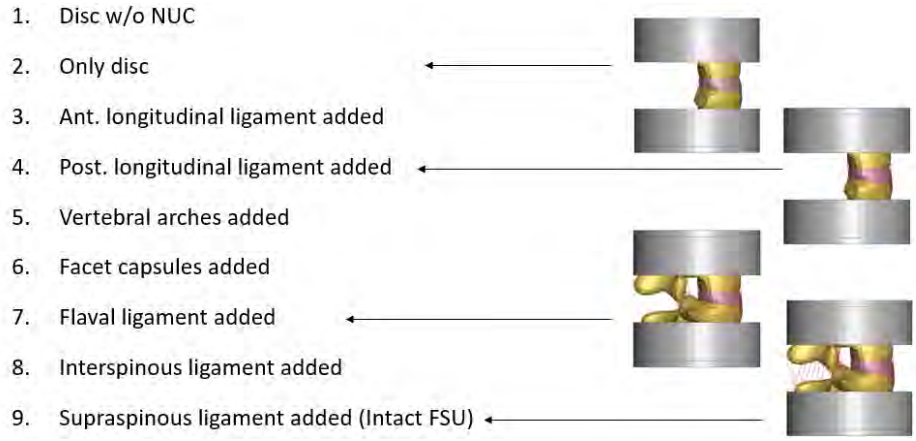

Fig. 2. Tuning of ligament initial unstretched length by adding one ligament or other anatomical structure at a time and comparing the force-deflection properties to [43,44]

Kinematic and kinetic validation of lumbar spine model

Kinematic and kinetic whole lumbar spine validation was performed by comparing the predictions from the complete lumbar spine model to two reference data sets [43,44]. The first reference test series, performed by Yamamoto *et al.* [49], included 10 lumbar spines from PMHSs aged between 25 and 63 years, but of unknown sex, stature and weight. The second reference test series, performed by Demetropoulos *et al.* [50], included 10 lumbar spines (8M/2F) from PMHSs with an average stature of 173 cm, an average weight of 73 kg and an average age of 60 years. As one of the data sets included specimens from both sexes and the PMHSs of the other dataset were of unknown sex, similar scaling as for the tuning of the ligament was used also for the validation simulations. Thus, the experimental results were compared to simulation results predicting the responses of a small female, an average sized female, an average sized male, and a large male.

In the Yamamoto *et al.* test series, the sacral vertebrae (and pelvis) were constrained in an epoxy block rigidly attached to the test table (see Fig. 3 left). At the superior end the L1 vertebrae was also potted in another epoxy block. The potting was modelled using an elastic material model with Young's modulus 2 GPa. The spine was connected to the potting using a penalty-based constraint (*CONSTRAINED_SHELL_IN_SOLID_PENALTY). Pure moment loads (extension-flexion, lateral bending and axial rotation) in steps of 2.5 Nm up to 10 Nm, were applied separately to the superior potting, and rotations were recorded at each vertebrae level. The superior potting was free to move in all directions, except the one currently being tested. Based on the figures and the description in [49], it was estimated that the spine was initially in a neutral (lordotic) position corresponding to a "LUMB_FLEX" parameter of -1.

In the Demetropoulos *et al.* test series, the T12 vertebrae were constrained in epoxy, rigidly attached to the test fixture (see Fig. 3 right). At the inferior end, L5 was also potted in epoxy. The potting material and connection between the potting and the spine were modelled in the same way as in the first load case. Compression (up to 6.5 mm), tension (up to 2.5 mm), anterior-posterior shear (up to 35 mm) and lateral shear (up to 13 mm) were applied to the inferior potting. The superior potting was constrained in all degrees of freedom. Based on the figures and the description in [50], it was estimated that the spine was in a neutral (lordotic) position corresponding to a "LUMB_FLEX" parameter of -1.

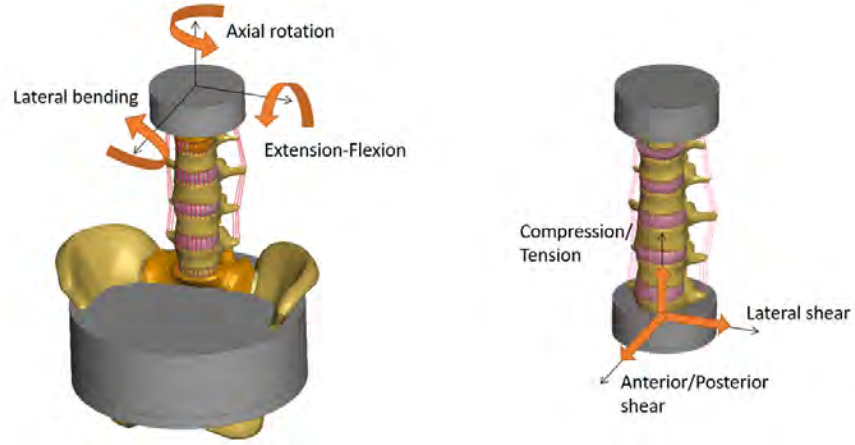

Fig. 3. Validation load cases: left, Yamamoto [49]; and right, Demetropoulos [50]. The orange arrows show the directions of the deformations applied.

Development of an Injury Risk Function

This study followed the guidelines defined by ISO/TC22/SC12/WG6 [51] and those presented in [52] on the construction of IRFs. In brief, an in-depth literature review was conducted to identify available datasets for reconstructions. The five test series selected, based on developed inclusion and exclusion criteria (see Appendix D), were those where two and three vertebral body FSUs were loaded in compression and combined flexion-compression until there was an endplate fracture or there was no injury when maximum load was applied. In total these contained 124 tests. The specimens were from donors with an average age of 46 years, but of unknown stature and weight. The proportion of male donors was 64%. Each of these tests were successfully reproduced with sub-models, based on the developed lumbar spine model (Fig. 4). Based on available information in each test series, the FSU simulation models were scaled to match the size of the vertebrae in each physical test. In test series [53] the endplate dimensions were used for scaling, in [54] the disc area, and in [55] the vertebrae body cross section. However, as several of the authors did not report how the measurements were taken a direct comparison with the FE model was not possible. Instead, it was assumed that the populations in each of the physical test series came from a normal (average sized) population. This means that the scaling factors were adjusted so within each test series, the average scale factor for female vertebrae was 1.00, and for male vertebrae 1.11 (according to the results in Appendix C). For the two last test series, [56] and [57], no vertebrae size information except sex was provided. For these tests all female vertebras were given a scale factor of 1.00 and all male vertebras a scale factor of 1.11. See additional information on test and reconstruction of these tests in Appendix E.

The injury to the physical FSUs was scored, either an endplate fracture or uninjured, and assigned censoring, exact or right (tests that did not result in any injury). Several candidate injury metrics were evaluated in initial simulations of frontal and side collisions. The inferior-superior compressive strain in the trabecular bone of the vertebrae body was found to be a good proxy for predicting endplate fractures and to be robust (other metrices indicated fracture also for tensile and shear loading of the lumbar spine).

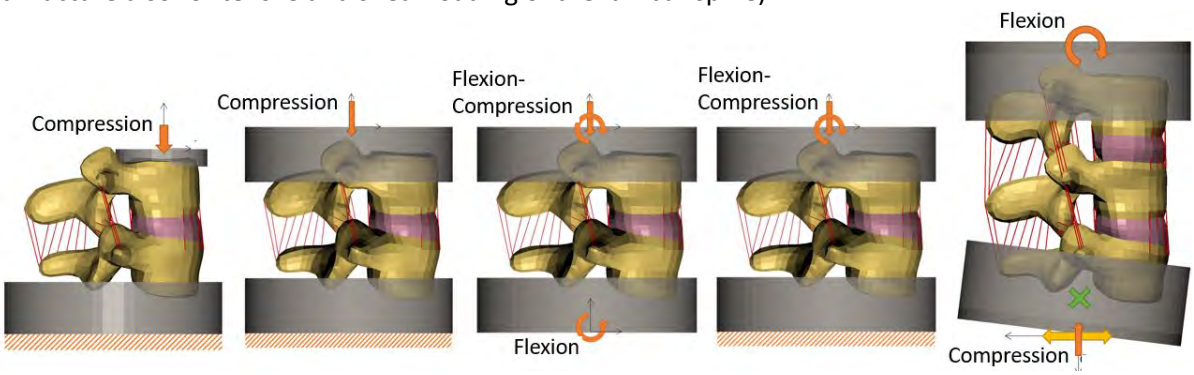

Fig. 4. FSU tests used to create IRF. From left to right: Brinckmann *et al.* [53], Duma *et al.* [56], Granhed *et al.* [57], Hutton and Adams [54], and Tushak *et al.* [55]. The orange arrows show the directions of the deformations applied. The green cross marks the rotation centre. The yellow arrow indicates that the end was free to translate in that DOF. The orange diagonal patterns mark that these ends were fixed.

Finally, the injury metric from the simulations and the injury scores from the original FSU tests were used in the construction of an IRF using parametric survival analysis using the R package "flexsurv". As part of the analysis, the effect of characteristics deemed important were studied using Cox regression for multiple covariates. The characteristics assessed were age, sex, and level of vertebrae (L1/L2 – ordinate 1, L2/L3 – ordinate 2, L3/L4 – ordinate 3, L4/L5 – ordinate 4, T12-L1-L2 – ordinate 5, L3-L4-L5 – ordinate 6). A p-value less than 0.05 inferred a statistical significance. In addition, an evaluation using DFBETA analysis was conducted to assess any presence of bias within the dataset. Overly influential observations were removed when DFBETA was outside of ±0.18. Thereafter the distribution assumptions were checked and evaluated to recommend the distribution that best predicts the true IRF. In short, the estimated risk curve for each of the three distributions (Weibull, log-normal and log-logistic) was compared with a spline function fitted to the simulation data. If any curve was substantially different from the spline, another distribution was considered. Then the distribution with the lowest Akaike Information Criterion (AIC) was selected. Finally, the 95% confidence interval of each IRF was calculated using the R package "*confint"*. The relative size of the confidence interval was defined as the width of the 95% confidence interval at a given injury risk relative to the value of the stimulus at this same injury risk and was assigned a quality index (four categories were used – good from 0 to 0.5, fair from 0.5 to 1.0, marginal from 1.0 to 1.5 and unacceptable over 1.5). These indexes were calculated at 5%, 25% and 50% risks of injury.

The final IRF was constructed using reconstructions of test according to TABLE II. Risk curves were constructed for ages 25-, 50- and 75-years for display.

TABLE II

THE FINAL DATASET USED IN THE DEVELOPMENT OF RISK CURVES

Information source	Loading speed	Type of loading	Number of tests/ injured (proportion males %)
Brinckmann (1989)	1 kN/s	Compression	41/41 (51)
Granhed (1989)	0.0002 m/s	Compression combined with flexion 5°, 10° or 15°	27/22 (67)
Hutton and Adams *et al.* (1982)	3 kN/s	Compression combined with initial flexion	24/24 (71)
Duma *et al.* (2006)	1 m/s	Compression	4/4 (100)
Tushak *et al.* (2022)	Compression 2.2-4.5 kN, Flexion 600 °/s	Compression followed by flexion	23/6 (70)

Evaluation of the Injury Risk Function

To evaluate the feasibility of the newly developed tissue based IRF, a reference test series was selected from literature. In the test series, performed by Ortiz-Paparoni, isolated lumbar spines were subjected to a combination of compression and flexion loading [58] (see Fig. 5). Complete spines from 32 (only Duke data used) male specimens (average height 177 cm, mass 81 kg, age 66 years) were tested. The sacrum and T12 were potted in firm plastic, modelled similarly as described in previous section. Different amount of flexion was assured by positioning the spine in three different curvatures: neutral, pre-flexed and pre-extended. The superior end was fixed, while the inferior end was moved with a constant velocity of 4 m/s. The fracture risk according to the newly developed IRF (for the average PMHS age of 66 years) was computed for the different combinations of axial loads and spine curvatures. The elements in the superior half of the L1 vertebrae had to be excluded from the risk calculation, as these interacted with the simplified and rigid T12 in a non-biomechanical fashion. The results were then compared to the force-based risk curve developed in [58].

Results from the IRF evaluation were converted into fracture risk using the IRF presented in this paper, an injury criteria and associated risk function suggested by [59] and risk function suggested by [60]. Finally, the estimated risks were compared to those presented in [58] for several applied loads.

Fig. 5. Evaluation of IRF according to test performed by Ortiz-Paparoni [58]

III. RESULTS

Development of a lumbar spine model

The final lumbar spine model, also morphed to an average-sized male and assembled into the seated VIVA+ 50F and 50M HBMs, can be seen in Fig. 6. The lumbar spine model consists of about 10,000 shell elements with an average side length of 3.2 mm, 15,000 solid elements with an average side length of 2.8 mm, and 300 beam elements. In the assembled model the lumbar lordosis is 4°, which can be compared the average 0–6° for seated occupants [61,62]. The lumbosacral slope is 161°, which can be compared to the average 165° for seated occupants [63].

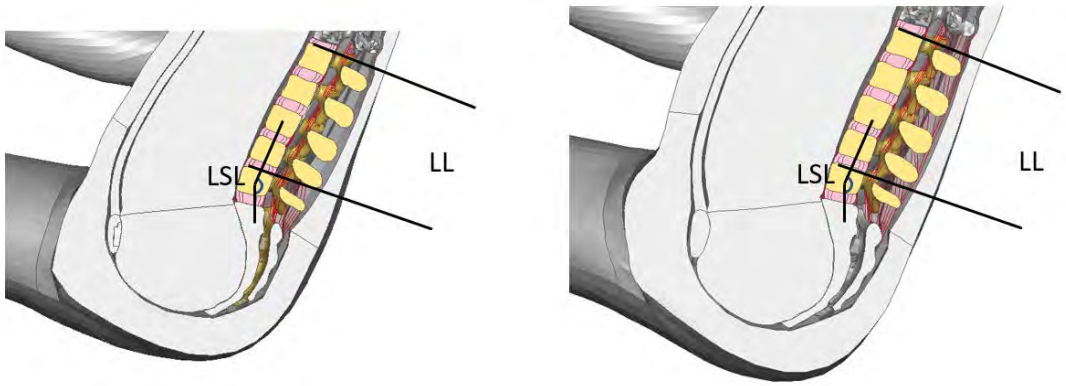

Fig. 6. The new lumbar spine model assembled into the VIVA+ 50F (left) and 50M (right) HBMs. The measurements defined in the figures are: Lumbar Lordosis angle (LL), measured from superior edge of the L1 vertebrae body to the superior edge of the L5 vertebrae body [61]; and LumboSacral Lordosis angle (LSL), defined as the angle between the line from L5 centre to L3 centre and the line between L5 centre and S1 centre [63].

Tuning of nucleus properties and ligament initial length

The L4-L5 FSU model predictions in compression and tension were compared to the reference data in Fig. 7. The predicted force-deflection response for compression was within the range of the physical tests, while the predicted stiffness was outside the reference data of the single experimental test series in tension.

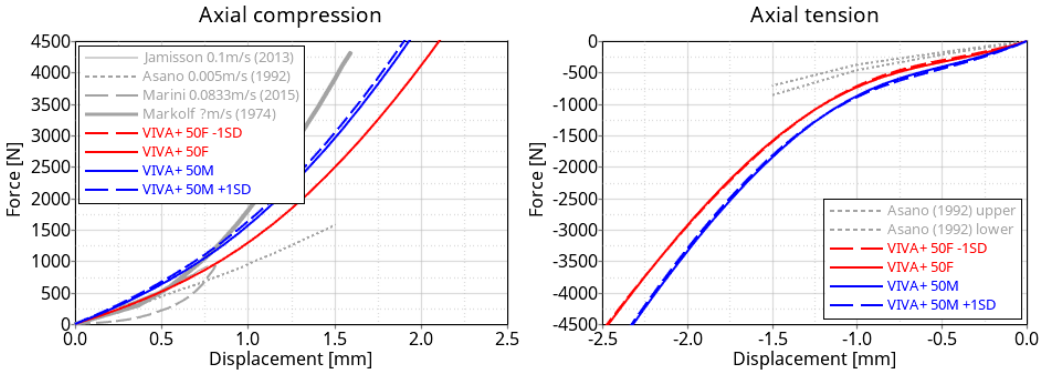

Fig. 7. Resulting force-deflection for L4-L5 FSU in axial compression (left) and axial tension (right) after nucleus pulposus material tuning, compared to [39-42].

The results from the ligament initial length tuning can be seen in Fig. 8 and Appendix B (see Fig. B 1 to Fig. B 8). Overall, the simulation predictions are within the range of the physical test results, in all of the nine steps. The major exceptions are the stiffness in lateral bending for the male vertebrae (too stiff all the way from bending of just the disc to bending of the complete FSU), and the stiffness in axial rotation for the small female vertebrae (too low in the complete FSU). Too reach these results, the initial pre-stretch/slack that were added to the ligaments were -1.5 mm for ALL, +1.5 mm for PLL, +2.0 mm for FC and FL and +5.0 mm for ISL and SSL. These offsets will be activated by setting the "LUMB_FLEX" parameter to -1.

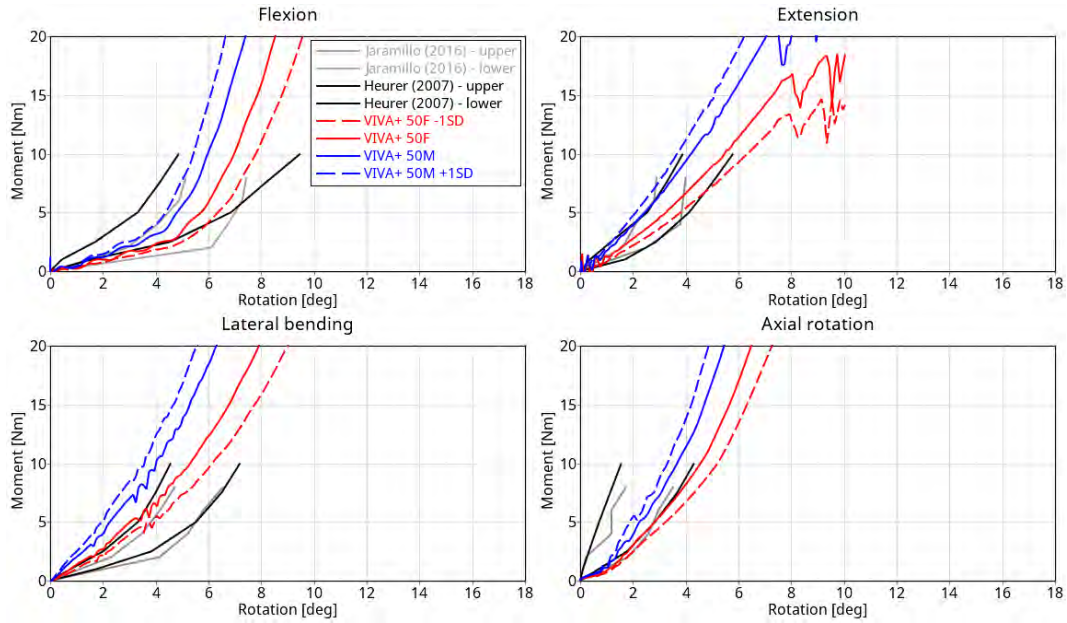

Fig. 8. Resulting moment-rotation for intact L4-L5 FSU in flexion (upper left), extension (upper right), lateral bending (lower left) and axial rotation (lower right), compared to [43,44]

Kinematic and kinetic validation of lumbar spine model

The results from the whole spine rotational kinematics and kinetics validation can be seen in Fig. 9. For flexion and extension, the model prediction lacks some of the neutral zone seen in the physical experiments, meaning that low moment responses are outside the experimental corridor. However, for higher moments (10Nm) the model responses are within or close to the corridor for all vertebrae sizes. Also, in lateral bending the model lacks some of the neutral zone seen in the physical experiments. At higher moments the responses of the female sized vertebras are in the middle of the corridor, while the male responses are at the border (stiffer response). For axial rotation the male responses are within (or at limit of) the experimental corridor, while the female responses are outside (on the weaker side). To check the assumption that the same ligament slack could be used at all lumbar spine levels, the spine kinematics and kinetics was also checked at each FSU level [49], see Appendix C.

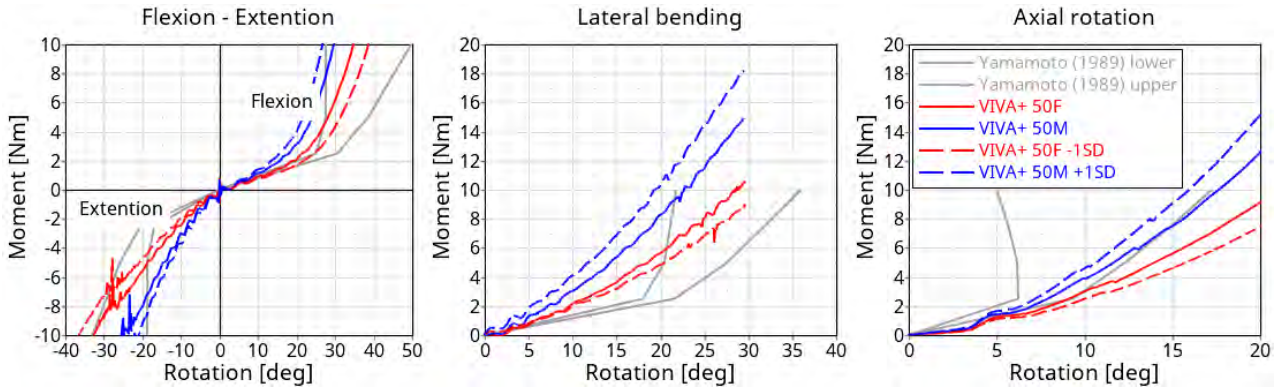

Fig. 9. Validation of whole spine rotational kinematics and kinetics [49], left: Flexion-Extension, mid: Lateral bending; and right: Axial rotation (same scale used in all plots for easier comparison of magnitudes)

The results from the whole spine translational kinematics and kinetics validation can be seen in Fig. 10. The compressive stiffness is within the experimental corridor for all vertebrae sizes, while the tensile response is outside (on the stiffer side). Both anterior and posterior shear stiffness is underpredicted, although the predicted anterior shear forces for large displacements (>35mm) are reasonable. The stiffness in lateral shear is also underpredicted, but only slightly for the male sized vertebras.

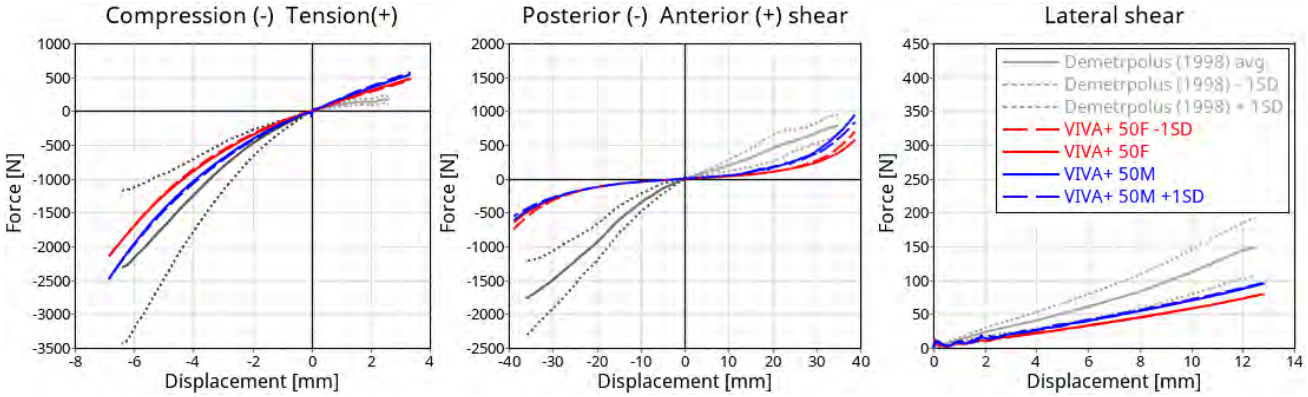

Fig. 10. Validation of whole spine translational kinematics and kinetics [50], left: Compression-Tension, mid: Posterior-Anterior shear; and right: Lateral shear (note that the scale for the lateral shear is different to the other two plots)

Development of an Injury Risk Function

Statistical analysis – the Cox regression analysis for any effects of characteristics deemed important (age, sex, and level of vertebrae) revealed that age was a significant predictor while sex and level of vertebrae were not significant. The final IRF should be constructed with age as a covariate. Further, an analysis on influential observations provided that no observations had to be removed prior to construction of the final IRF.

Injury risk function – an fracture IRF recommended for use with the new lumbar spine model was developed using the maximum inferior-superior compressive strain in the trabecular bone. Curves for a model representative of ages 25-, 50- and 75-years are provided in Fig. 11.

Equation 1, with the coefficients given in Table III, provides the lumbar spine IRF for the new lumbar spine model. The risk according to the log-normal distribution is:

$$\text{Risk} = \frac{1}{2} + \frac{1}{2}\text{erf}\left(\frac{\ln(\text{injury criteria}) - (\beta_1 + \text{age} * \text{coef}_{\text{age}})}{\sqrt{2 * (\exp(\beta_2))^2}}\right) \quad (1)$$

Table III

DISTRIBUTION AND PARAMETERS FOR THE INJURY RISK FUNCTION RECOMMENDED FOR THE NEW LUMBAR SPINE MODEL

Injury risk	Injury criteria	Distribution	$\boldsymbol{\beta_1}$	$\boldsymbol{\beta_2}$	$\boldsymbol{coef_{age}}$
Fracture	Strain	Log-normal	-2.833	-0.885	-0.0149

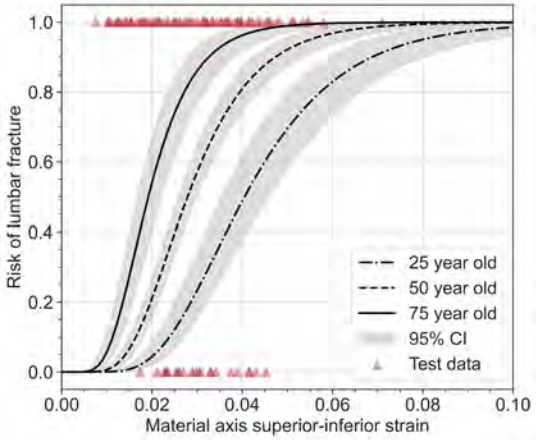

Fig. 11. Injury risk curves recommended for use with the new lumbar spine model and for ages 25, 50 and 75 years.

TABLE IV provides the confidence limits and the quality index that correspond to 5%, 25% and 50% risks of injury from the recommended curves.

TABLE IV
INJURY RISKS AND QUALITY INDEX FOR RISK CURVES FOR AGE 50

Risk (%)	Mean inferior-superior compressive strain	Confidence limit, lower	Confidence limit, upper	Confidence error	Grade
5	0. 014	0. 013	0. 016	0.23	Good
25	0. 029	0. 027	0. 032	0.16	Good
50	0. 028	0. 026	0. 030	0.16	Good

Evaluation of the Injury Risk Function

Selected results from the IRF evaluation can be seen in Fig. 12. A comparison to the Ortiz-Paparoni risk curve shows that the simulation model and the new strain based IRF somewhat overpredicts the fracture risk, as several of the symbols corresponding to simulation results are located to the left of the force-based risk curve. Comparing the three spine curvatures, the pre-extended spine model predicts the lowest risk, and the pre-flexed spine model predicts the highest risk. In all cases the highest strain was in the L1 vertebrae (lower half). For low risk levels (<50%) the tissue base risk curve predicts higher risk than the force-based curves, while for higher risk levels (>50-80%) the force based curves predicts higher risk than the tissue based curve.

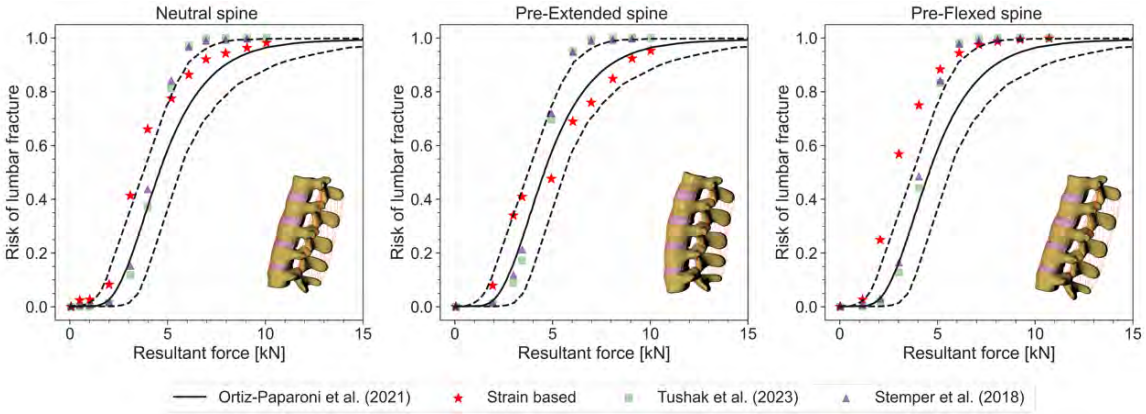

Fig. 12. Results from evaluation of IRF according to Ortiz-Paparoni [58], where the black lines represents the force-based injury risk from the PMHS tests (combination of spine curvatures), and the symbols represent the estimated injury risk from the simulation model for the neutral, pre-flexed and pre-extended spines using the IRF presented in this paper (Strain based), an injury criteria and associated risk function suggested by Tushak *et al.* [59] and risk function suggested by Stemper *et al.* [60].

IV. DISCUSSION

The current study presents the development and validation of a lumbar spine FE model with an associated tissue based IRF for the assessment of lumbar spine compression fractures. The model is primarily intended for injury prevention applications in the traffic environment but might also be useful for other applications.

The modelling of the disc has been shown to be important for the loading of the endplate and the trabecular bone underneath the endplate [64]. In the current study the annulus was modelled based on published material parameters, whereas the nucleus was tuned to FSU compression test data. While the area of the nucleus was matched to literature sources, it is also important that the load sharing between the nucleus and anulus is correct, as this will contribute to the fracture onset and location. While no data was found to directly validate the load sharing in compression, it was indirectly checked in the first two steps of the comparison to the FSU tests [43,44] used for ligament and nucleus tuning. In the first step the rotational stiffness was measured without the nucleus (only the anulus holding the vertebras together), while in the second step the nucleus was also included, see Appendix B. In all loadings except lateral bending for the male sized vertebrae the predicted results were within the experimental results. This indicates that the annulus properties are reasonable, while the nucleus contribution to lateral bending is too high in the model.

Further, it has also been shown that the disc is highly strain rate dependent [38], which might also influence the vertebrae fracture onset and location. In the current study neither the annulus nor the nucleus was modelled to include strain rate dependency. Also, material tuning of the nucleus was done based on quasi-static (0.005 m/s) to low-speed (0.1 m/s) dynamic tests. Previous studies indicate that the disc stiffness might increase markedly around a loading speed of 1 m/s [65]. Therefore, there is a risk that the current model is too flexible at loading rates of 1 m/s and above.

It was not possible to increase the axial stiffness without, at the same time, affecting the rotational stiffnesses and in particular the lateral bending stiffness. As seen in Fig. B 2, the lateral bending stiffness for an FSU without any ligaments (only the disc contributes to the stiffness) is already too high compared to the experimental results, and this too high stiffness is carried all the way to the intact FSU in Fig. 8. It should be noted, however, that the physical rotational stiffness tests used for ligament tuning were performed at low loading speeds (1-2.8°/s) and thus, for a higher speed, in line with a 1 m/s axial compression test, the rotational stiffness might be significantly higher.

In the IRF evaluation phase it was noticed that L1 interacted with the rigid T12 (from the original VIVA+ model) in an unphysical way. As the rigid T12 could not deform as a result of the increased pressure in the disc during loading, L1 showed additional, unphysical deformations and too high strain levels. It is thus recommended for future studies to model T12 in detail as well, if all vertebrae of the lumbar spine are to be included in the calculation of injury risk. In the current study, the solution was to remove the superior half of L1 from the injury risk calculations.

The parameter "LUMB_FLEX" was introduced to account for ligament initial slack or pre-stretch that depends on the curvature of the spine. If this effect was disregarded, the stiffness in flexion would be much too high. This was also noted for the Chazal ligament data (used for the current model) in a study comparing the influence of ligament mechanical properties [66]. In the tuning, all ligaments posterior of the joint centre of rotation (approximately at the rear 1/3 of the disc) got a positive offset (initial slack) in the tuning phase, while the ALL ligament got a negative offset (initial pre-stretch). The further away from the rotation centre, the larger the offset, with the largest offset (+5 mm) occurring for the ISL and SSL ligaments. Thus, it was hypothesised (as it was not reported) that the FSUs in the physical tests used for ligament initial length tuning were in a lordotic posture, slacking the posterior ligaments. Flexing the spine from this position will gradually remove the initial slack. In [61,63] the authors report an average change in lumbar flexion of about 8° per motion segment when transitioning from standing to sitting (in a vehicle seat). This rotation roughly matches the removal of the initial slack and thus it is recommended to use LUMB_FLEX=-1 for a standing posture, and LUMB_FLEX=0 for a seated posture.

One limitation in the ligament tuning and validation of the lumbar spine FE model is that the rotational tests could only be compared up to 10 Nm (maximum load in physical experiments), which is very low compared to flexion moments at fracture ranging up to 300+ Nm [58]. It should be noted that the Demetropoulos *et al.* [50] test series included rotational test up to failure, in flexion, extension and lateral bending, in addition to the translational loads used for the validation in this study. While the stiffness in flexion reported by Demetropoulos

et al. matched the Yamamoto *et al.* [49] results, the reported stiffnesses in extension and lateral bending were much higher. After comparing Demetropoulos *et al.* extension and lateral bending results to the lumbar spine physical range of motion (RoM) [67] it was concluded that the stiffness in these directions were unrealistic (about 150 Nm would be required to reach the RoM), and thus these tests were not used for model validation. It was hypothesised that the lumbar spines tests in [50] might have started from a highly lordotic curvature, which could potentially explain the difference in results compared to other studies.

The quality of the data used in the construction of the IRF were deemed fair. The age was distributed evenly between the two sexes in the dataset and, e.g. the securing of the vertebrae bodies to the loading devices and the loading conditions were well described and could be modelled with fair accuracy.

Age was the only significant parameter affecting the prediction of the inferior-superior compressive strains according to the Cox analysis. Thus, only the covariate age was used in the construction of the final IRF.

In this study, data from five source were reproduced, and used in the construction of risk functions. By using many data sources, potential errors in the setups (physical or simulation version) becomes less influential. However, the age, failure load and estimated strain at failure distributions, see Fig. 13, for each data source reveal that Hutton and Adam [54] tested several rather stronger specimens (both failure loads and estimated strains were higher than average), Duma *et al.* [56] tested at higher speed than used in the other sources (failure at higher loads). Age was rather uniform. Exceptions were the large proportion of the specimens from younger males included in tests by Hutton and Adam [54] and Granhed *et al.* [57] and large proportion of the specimens from older females included in tests by Granhed *et al.* [57].

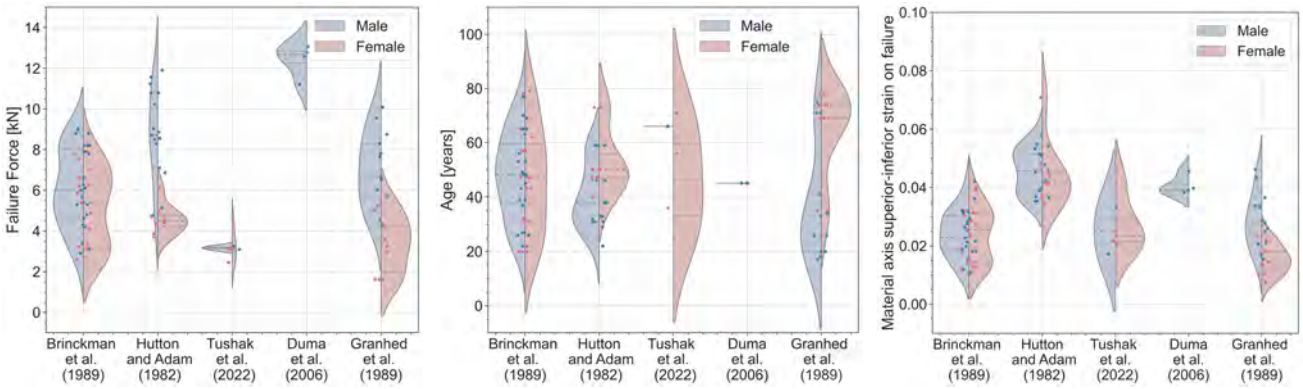

Fig. 13. Summary statistics on the data sources used to construct the IRF.

All left censored data that potentially could have been included in the development of the IRF in this study were dropped, as the number of cases with exact data was deemed sufficient.

Several types of lumbar vertebrae body compression fractures occur in vehicle crashes, including wedge fractures, burst fractures and biconcave fractures. Several studies have investigated the mechanisms of lumbar spine fractures and many have found evidence that fracture initiates from the endplate [68,69]. Endplate injuries may well occur in vehicle crashes, although not sufficiently detailed in vehicle crash databases, and may precede the fractures of the trabecular and cortical bones. The injury metric chosen for the IRF presented in this study was the compressive strain in the local vertebrae superior-inferior direction, measured in the solid elements representing the trabecular bone of the vertebrae body. Other metrics, such as effective plastic strain or 1st principal strain in the cortical bone or the endplates, were considered but were discarded as they could not separate between compressive and tensile loading, while the IRF should only predict risk for compression fractures.

There were several reasons for selecting data on lumbar spine endplate fractures for the construction of our IRF. Firstly, one of the most common types of compression fracture only involves the failure of the upper endplate of the vertebra [70,71] . Secondly, these endplate fractures may lead to long term pain and suffering [72]. Thirdly, the developed model does not include element erosion and consequently the model response is reliable until first fracture.

The choice of evaluating the superior-inferior strain in the trabecular bone instead of, for example, the endplates was due to several reasons. First, as the endplates were modelled using shell elements, the out of plane stresses (corresponding to the superior-inferior direction) are by element design not computed. Secondly, tests

on lumbar spine segments were undertaken with the aim of measuring the change in pressure in the trabecular bone during a burst fracture [68,69] and reported an increase in internal pressure in the vertebrae after an onset of endplate failure. In the current study, it was hypothesised that fracture of the endplate occurs at about the same time as in the underlying trabecular bone (supporting the endplates), and thus the fracture in the trabecular bone could be used as a proxy for endplate fractures. Similarly, it can be hypothesised that inferior-superior compressive strain in the trabecular bone of the vertebrae body can also be a fair proxy for the wedge and burst fractures in the lumbar spine.

Another limitation was that the IRF evaluation indicated that the model, together with the associated IRF, overpredicted the injury risk, at least for some spine curvatures. There could be many reasons for this, from improper model deformation at high loads, or improper load distribution in the disc (discussed in previous paragraphs), to unknown boundary conditions that affected the simulations of the FSU tests used to develop the IRF. Also, as the criteria for the IRF was the initial fracture of the end plate, and not the complete fracture of the vertebrae body, means that the predicted fracture load will be somewhat lower. Hence, the evaluation of the IRF carried out in this study is deemed to be inclusive and it is judged that the current model, together with the associated IRF, can be used to estimate the risk for compressive fractures in the lumbar spine, with the knowledge that these estimates might be somewhat conservative. To address some of these limitations, future validation should preferably include additional tests with combined loading at higher loads, and higher loading speeds [55].

The lumbar spine model presented in this study was integrated into the VIVA+ HBMs, which can be downloaded at openvt.eu [73].

V. CONCLUSIONS

A new open-source finite element lumbar spine model was developed and validated together with an associated tissue-based injury risk function. A parameter was introduced assigning ligament slack/pre-stretch based on initial spine curvature. The model was shown to predict kinematic and kinetic reasonably, with best performance for axial compression and flexion. The tissue-based injury risk function, based on reconstructions of 124 FSU tests, showed good statistical properties. The evaluation of the injury risk function indicated that the fracture risk was somewhat overpredicted. Despite this, it is judged that the current model, together with the associated IRF, can be used to estimate the risk for compressive fractures in the lumbar spine.

VI. ACKNOWLEDGEMENTS

This work was carried out at SAFER, Vehicle and Traffic Safety Centre at Chalmers University of Technology, Gothenburg, Sweden, and was funded by the OSCCAR project, which has received funding from the European Union Horizon 2020 Research and Innovation Programme under Grant Agreement No. 768947, and by the SAFE-UP project, which has received funding from the European Union Horizon 2020 Research and Innovation Programme under Grant Agreement No. 861570. The content of this paper does not reflect the official opinion of the European Union. Responsibility for the information and assessments stated therein lies totally with the authors. The simulations were enabled by resources provided by the National Academic Infrastructure for Supercomputing in Sweden (NAISS) at Chalmers partially funded by the Swedish Research Council through grant agreement no. 2022-06725.

VII. REFERENCES

[1] Huelke, D.F., Mackay, G.M., and Morris, A. Vertebral column injuries and lap-shoulder belts. *Journal of Trauma and Acute Care Surgery*, 1995. 38(4): p. 547-556

[2] Pintar, F.A., Yoganandan, N., Maiman, D.J., Scarboro, M., and Rudd, R.W. Thoracolumbar spine fractures in frontal impact crashes. *Proceedings of Annals of Advances in Automotive Medicine/Annual Scientific Conference*, 2012.

[3] Adolph, T., Wisch, M., et al. Analyses of thoracic and lumbar spine injuries in frontal impacts. *Proceedings of IRCOBI Conference on Biomechanics of Impacts*, 2013.

[4] Kaufman, R.P., Ching, R.P., et al. Burst fractures of the lumbar spine in frontal crashes. *Accident Analysis & Prevention*, 2013. 59: p. 153-163

[5] Doud, A.N., Weaver, A.A., et al. Has the incidence of thoracolumbar spine injuries increased in the United States from 1998 to 2011? *Clinical Orthopaedics and Related Research®*, 2015. 473: p. 297-304

[6] Jakobsson, L., Björklund, M., and Westerlund, A. Thoracolumbar spine injuries in car crashes. *Proceedings of International Conference on the Biomechanics of Injury*, 2016.

[7] Shaikh, J., Thathia, H., and Lubbe, N. Lumbar spine injuries in motor vehicle crashes. *Proceedings of IRCOBI Asia Conference*, 2020.
[8] Begeman, P.C., King, A.I., and Prasad, P. Spinal loads resulting from-Gx acceleration. 1973, SAE Technical Paper.
[9] Patrick, L. and Levine, R. Injury to unembalmed belted cadavers in simulated collisions. 1975, SAE Technical Paper.
[10] Rouhana, S.W., Bedewi, P.G., et al. Biomechanics of 4-point seat belt systems in frontal impacts. *Stapp car crash journal*, 2003. 47: p. 367
[11] Richardson, R., Donlon, J.-P., et al. Kinematic and injury response of reclined PMHS in frontal impacts. *Stapp car crash journal*, 2020. 64: p. 83-153
[12] Richardson, R., Jayathirtha, M., et al. Thoracolumbar spine kinematics and injuries in frontal impacts with reclined occupants. *Traffic injury prevention*, 2020. 21(sup1): p. S66-S71
[13] Katsuhara, T., Takahira, Y., Hayashi, S., Kitagawa, Y., and Yasuki, T. Analysis of driver kinematics and lower thoracic spine injury in world endurance championship race cars during frontal impacts. *SAE International journal of transportation safety*, 2017. 5(1): p. 120-132
[14] Boyle, K.J., Reed, M.P., Zaseck, L.W., and Hu, J. A human modelling study on occupant kinematics in highly reclined seats during frontal crashes. *Proceedings of the International Research Conference on the Biomechanics of Impact, IRCOBI, Florence, Italy, 11th September-13th September. IRC-19-43*, 2019.
[15] Rawska, K., Gepner, B., et al. Submarining sensitivity across varied anthropometry in an autonomous driving system environment. *Traffic injury prevention*, 2019. 20(sup2): p. S123-S127
[16] Butala, K., Gotwals, D., Tangirala, R., and Shanks, K. Occupant Behavior in Small Front Overlap Event – A Parametric Study. *Proceedings of 23st International Technical Conference on the Enhanced Safety of Vehicles*, 2013. Seoul, Republic of Korea
[17] Shigeta, K., Kitagawa, Y., and Yasuki, T. Development of next generation human FE model capable of organ injury prediction. *Proceedings of The 21st Annual Enhanced Safety of Vehicles*, 2009. Stuttgart, Germany
[18] Gayzik, F.S., Moreno, D.P., Vavalle, N.A., Rhyne, A.C., and Stitzel, J.D. Development of a full human body finite element model for blunt injury prediction utilizing a multi-modality medical imaging protocol. *Proceedings of 12th International LS-DYNA User Conference*, 2012.
[19] Pipkorn, B., Östh, J., et al. Validation of the SAFER Human Body Model Kinematics in Far-Side Impacts. *Proceedings of the International IRCOBI Conference*, 2021. Online
[20] John, J., Klug, C., Kranjec, M., Svenning, E., and Iraeus, J. Hello, world! VIVA+: A human body model lineup to evaluate sex-differences in crash protection. *Frontiers in bioengineering and biotechnology*, 2022. 10
[21] Tushak, S.K., Gepner, B.D., Pipkorn, B., and Kerrigan, J.R. Evaluation of the GHBMC lumbar spine in sub-injurious and injurious loading. *Proceedings of International Research Council on Biomechanics of Injury*, 2022.
[22] Yoganandan, N., Moore, J., et al. Human lumbar spinal column injury criteria from vertical loading at the base: Applications to military environments. *Journal of the Mechanical Behavior of Biomedical Materials*, 2020: p. 103690
[23] R Core Team. R: A language and environment for statistical computing. 2022, R Foundation for Statistical Computing: Vienna, Austria.
[24] Gayzik, F., Hamilton, C.A., et al. A Multi-Modality Image Data Collection Protocol for Full Body Finite Element Model Development. 2009, SAE Technical Paper.
[25] Kopperdahl, D.L., Morgan, E.F., and Keaveny, T.M. Quantitative computed tomography estimates of the mechanical properties of human vertebral trabecular bone. *Journal of orthopaedic research*, 2002. 20(4): p. 801-805
[26] Ulrich, D., Van Rietbergen, B., Laib, A., and Ruegsegger, P. The ability of three-dimensional structural indices to reflect mechanical aspects of trabecular bone. *Bone*, 1999. 25(1): p. 55-60
[27] Khor, F., Cronin, D.S., Watson, B., Gierczycka, D., and Malcolm, S. Importance of asymmetry and anisotropy in predicting cortical bone response and fracture using human body model femur in three-point bending and axial rotation. *Journal of the mechanical behavior of biomedical materials*, 2018. 87: p. 213-229
[28] Wu, Y., Loaiza, J., Banerji, R., Blouin, O., and Morgan, E. Structure-function relationships of the human vertebral endplate. *JOR spine*, 2021. 4(3): p. e1170
[29] Cassidy, J., Hiltner, A., and Baer, E. Hierarchical structure of the intervertebral disc. *Connective tissue research*, 1989. 23(1): p. 75-88
[30] Holzapfel, G.A., Schulze-Bauer, C., Feigl, G., and Regitnig, P. Single lamellar mechanics of the human lumbar anulus fibrosus. *Biomechanics and modeling in mechanobiology*, 2005. 3(3): p. 125-140
[31] Panzer, M.B. and Cronin, D.S. C4–C5 segment finite element model development, validation, and load-sharing investigation. *Journal of biomechanics*, 2009. 42(4): p. 480-490
[32] Chazal, J., Tanguy, A., et al. Biomechanical properties of spinal ligaments and a histological study of the supraspinal ligament in traction. *Journal of biomechanics*, 1985. 18(3): p. 167-176
[33] Mattucci, S.F. and Cronin, D.S. A method to characterize average cervical spine ligament response based on raw data sets for implementation into injury biomechanics models. *Journal of the mechanical behavior of biomedical materials*, 2015. 41: p. 251-260

[34] Nolte, L.P., Panjabi, M., and Oxland, T. Biomechanical properties of lumbar spinal ligaments. *Clinical implant materials, advances in biomaterials*, 1990. 9: p. 663-668
[35] Smit, T.H., Odgaard, A., and Schneider, E. Structure and function of vertebral trabecular bone. *Spine*, 1997. 22(24): p. 2823-2833
[36] Edwards, W.T., Zheng, Y., Ferrara, L.A., and Yuan, H.A. Structural features and thickness of the vertebral cortex in the thoracolumbar spine. *Spine*, 2001. 26(2): p. 218-225
[37] Alonso, F. and Hart, D., "Encyclopedia of the Neurological Sciences", pages 724-729, Elsevier: 32 Jamestown Road, London NW1 7BY, UK, 2014
[38] Newell, N., Little, J., et al. Biomechanics of the human intervertebral disc: A review of testing techniques and results. *Journal of the mechanical behavior of biomedical materials*, 2017. 69: p. 420-434
[39] Jamison, D., Cannella, M., Pierce, E.C., and Marcolongo, M.S. A comparison of the human lumbar intervertebral disc mechanical response to normal and impact loading conditions. *Journal of Biomechanical Engineering*, 2013. 135(9)
[40] Asano, S., Kaneda, K., Umehara, S., and Tadano, S. The Mechanical Properties of the Human L4–5 Functional Spinal Unit During Cyclic Loading: The Structural Effects of the Posterior Elements. *Spine*, 1992. 17(11): p. 1343-1352
[41] Marini, G., Studer, H., Huber, G., Püschel, K., and Ferguson, S.J. Geometrical aspects of patient-specific modelling of the intervertebral disc: Collagen fibre orientation and residual stress distribution. *Biomechanics and modeling in mechanobiology*, 2016. 15(3): p. 543-560
[42] Markolf, K.L. and Morris, J.M. The structural components of the intervertebral disc: a study of their contributions to the ability of the disc to withstand compressive forces. *JBJS*, 1974. 56(4): p. 675-687
[43] Heuer, F., Schmidt, H., Klezl, Z., Claes, L., and Wilke, H.-J. Stepwise reduction of functional spinal structures increase range of motion and change lordosis angle. *Journal of biomechanics*, 2007. 40(2): p. 271-280
[44] Jaramillo, H.E., Puttlitz, C.M., McGilvray, K., and García, J.J. Characterization of the L4–L5–S1 motion segment using the stepwise reduction method. *Journal of Biomechanics*, 2016. 49(7): p. 1248-1254
[45] Berry, J.L., Moran, J.M., Berg, W.S., and Steffee, A.D. A morphometric study of human lumbar and selected thoracic vertebrae. *Spine*, 1987. 12(4): p. 362-367
[46] Gilad, I. and Nissan, M. A study of vertebra and disc geometric relations of the human cervical and lumbar spine. *Spine*, 1986. 11(2): p. 154-157
[47] Scoles, P.V., Linton, A.E., Latimer, B., Levy, M.E., and Digiovanni, B.F. Vertebral body and posterior element morphology: the normal spine in middle life. *Spine*, 1988. 13(10): p. 1082-1086
[48] Zhou, S., McCarthy, I., McGregor, A., Coombs, R., and Hughes, S. Geometrical dimensions of the lower lumbar vertebrae–analysis of data from digitised CT images. *European Spine Journal*, 2000. 9: p. 242-248
[49] Yamamoto, I., Panjabi, M.M., Crisco, T., and Oxland, T. Three-dimensional movements of the whole lumbar spine and lumbosacral joint. *Spine*, 1989. 14(11): p. 1256-1260
[50] Demetropoulos, C.K., Yang, K.H., Grimm, M.J., Khalil, T.B., and King, A.I. Mechanical properties of the cadaveric and Hybrid III lumbar spines. *SAE transactions*, 1998: p. 2862-2871
[51] ISO/TR 12350:2013. Road vehicles -- Injury risk curves for the evaluation of occupant protection in side impact tests. 2013: Geneva, Switzerland.
[52] Petitjean, A. and Trosseille, X. Statistical simulations to evaluate the methods of the construction of injury risk curves. 2011, SAE Technical Paper.
[53] Brinckmann, P., Biggemann, M., and Hilweg, D. Prediction of the compressive strength of human lumbar vertebrae. *Clinical Biomechanics*, 1989. 4: p. iii-27
[54] Hutton, W. and Adams, M. Can the lumbar spine be crushed in heavy lifting? *Spine*, 1982. 7(6): p. 586-590
[55] Tushak, S.K., Donlon, J.P., et al. Failure tolerance of the human lumbar spine in dynamic combined compression and flexion loading. *Journal of Biomechanics*, 2022. 135: p. 111051
[56] Duma, S.M., Kemper, A.R., McNeely, D.M., Brolinson, P.G., and Matsuoka, F. Biomechanical response of the lumbar spine in dynamic compression. *Biomedical sciences instrumentation*, 2006. 42: p. 476-481
[57] Granhed, H., Jonson, R., and Hansson, T. Mineral content and strength of lumbar vertebrae A cadaver study. *Acta Orthopaedica Scandinavica*, 1989. 60(1): p. 105-109
[58] Ortiz-Paparoni, M., Op't Eynde, J., et al. The human lumbar spine during high-rate under seat loading: a combined metric injury criteria. *Annals of biomedical engineering*, 2021. 49: p. 3018-3030
[59] Tushak, S.K., Gepner, B.D., et al. Human lumbar spine injury risk in dynamic combined compression and flexion loading. *Annals of Biomedical Engineering*, 2023: p. 1-10
[60] Stemper, B.D., Chirvi, S., et al. Biomechanical tolerance of whole lumbar spines in straightened posture subjected to axial acceleration. *Journal of Orthopaedic Research®*, 2018. 36(6): p. 1747-1756
[61] Nishida, N., Izumiyama, T., et al. Changes in the global spine alignment in the sitting position in an automobile. *The Spine Journal*, 2020. 20(4): p. 614-620
[62] Izumiyama, T., Nishida, N., et al. Analysis of individual variabilities for lumbar and pelvic alignment in highly reclined seating postures and occupant kinematics in a collision. *Proceedings of the International IRCOBI Conference*, 2022.

[63] De Carvalho, D.E., Soave, D., Ross, K., and Callaghan, J.P. Lumbar spine and pelvic posture between standing and sitting: a radiologic investigation including reliability and repeatability of the lumbar lordosis measure. *Journal of Manipulative and Physiological Therapeutics*, 2010. 33(1): p. 48-55

[64] Wagnac, E., Arnoux, P.-J., Garo, A., and Aubin, C.-E. Finite element analysis of the influence of loading rate on a model of the full lumbar spine under dynamic loading conditions. *Medical & biological engineering & computing*, 2012. 50(9): p. 903-915

[65] Kemper, A.R., McNally, C., and Duma, S.M. The influence of strain rate on the compressive stiffness properties of human lumbar intervertebral discs. *Biomedical sciences instrumentation*, 2007. 43: p. 176-181

[66] Naserkhaki, S., Arjmand, N., Shirazi-Adl, A., Farahmand, F., and El-Rich, M. Effects of eight different ligament property datasets on biomechanics of a lumbar L4-L5 finite element model. *Journal of biomechanics*, 2018. 70: p. 33-42

[67] Arshad, R., Pan, F., Reitmaier, S., and Schmidt, H. Effect of age and sex on lumbar lordosis and the range of motion. A systematic review and meta-analysis. *Journal of biomechanics*, 2019. 82: p. 1-19

[68] Yoganandan, N., Larson, S.J., et al. Correlation of microtrauma in the lumbar spine with intraosseous pressures. *Spine*, 1994. 19(4): p. 435-440

[69] Ochia, R.S. and Ching, R.P. Internal pressure measurements during burst fracture formation in human lumbar vertebrae. *Spine*, 2002. 27(11): p. 1160-1167

[70] Denis, F. The three column spine and its significance in the classification of acute thoracolumbar spinal injuries. *spine*, 1983. 8(8): p. 817-831

[71] Denis, F. Spinal instability as defined by the three-column spine concept in acute spinal trauma. *Clinical Orthopaedics and Related Research (1976-2007)*, 1984. 189: p. 65-76

[72] Van Dieën, J., Weinans, H., and Toussaint, H. Fractures of the lumbar vertebral endplate in the etiology of low back pain: a hypothesis on the causative role of spinal compression in aspecific low back pain. *Medical hypotheses*, 1999. 53(3): p. 246-252

[73] John, J., Poojary, Y., Jaber, L., Thomson, R., and Iraeus, J. VIVA+ 2.0.0 Beta. 2023.

VIII. APPENDIX A – VERTEBRAE BODY SIZE COMPARISON TO LITERATURE

Fig. A 1. VIVA+ vertebrae body height compared to literature sources

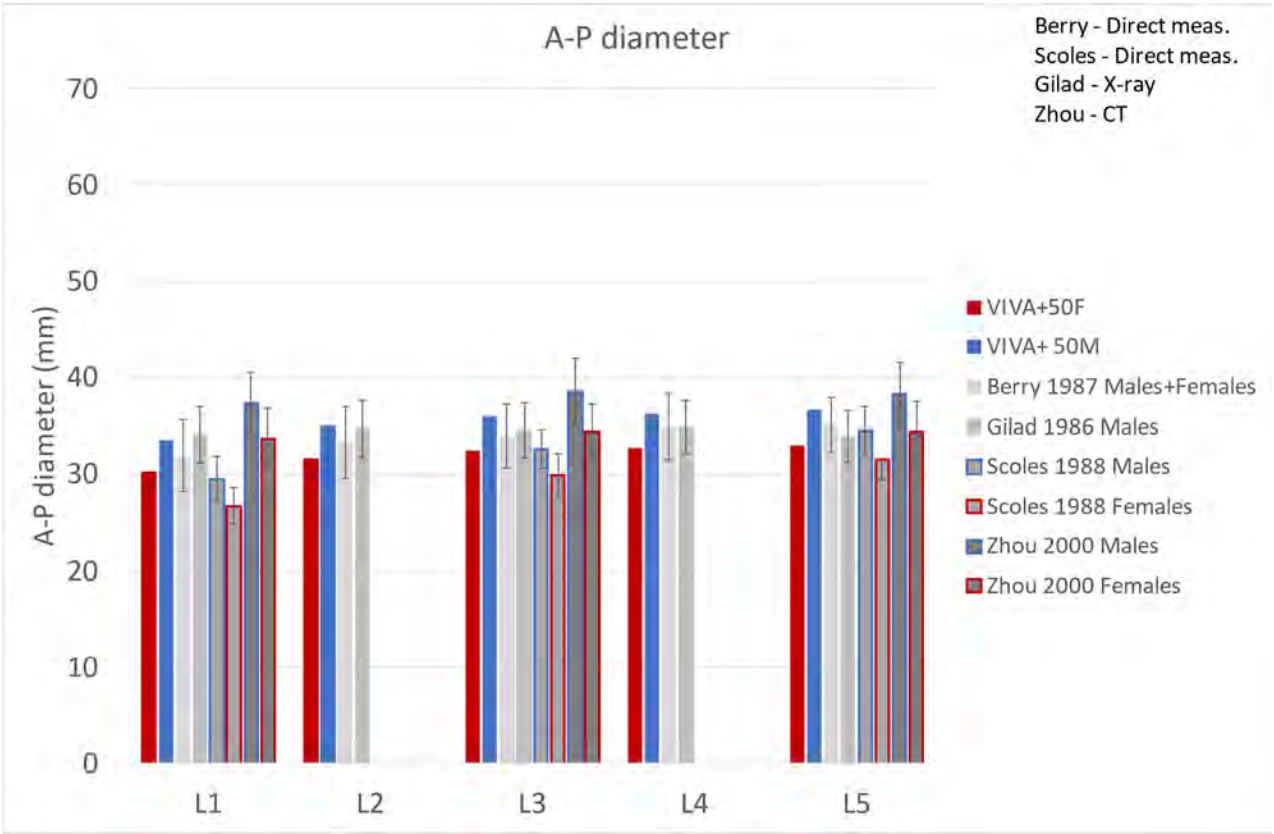

Fig. A 2. VIVA+ vertebrae body anterior-posterior diameter compared to literature sources

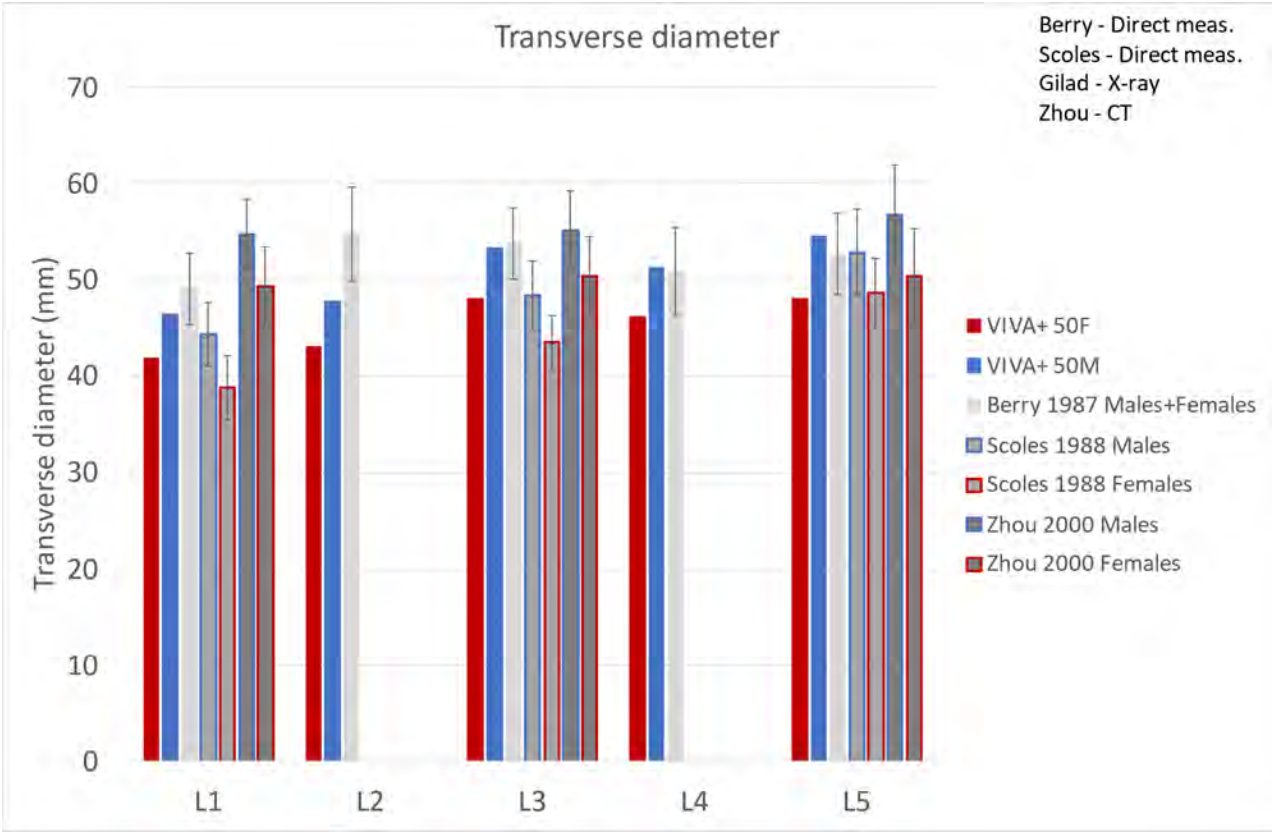

Fig. A 3. VIVA+ vertebrae body transverse diameter compared to literature sources

IX. Appendix B – Detailed results from ligament initial length tuning

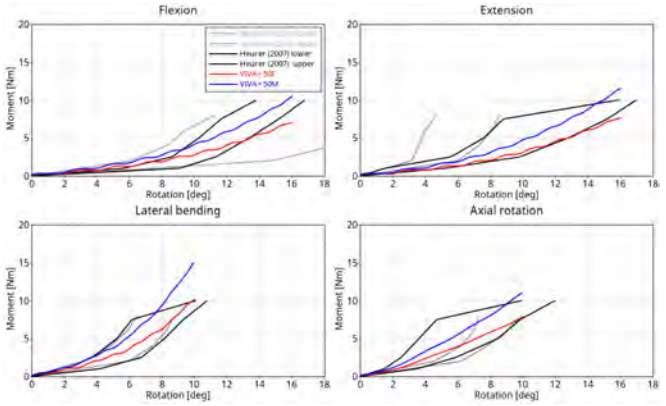

Fig. B 1. Step 1 – disc w/o NUC.

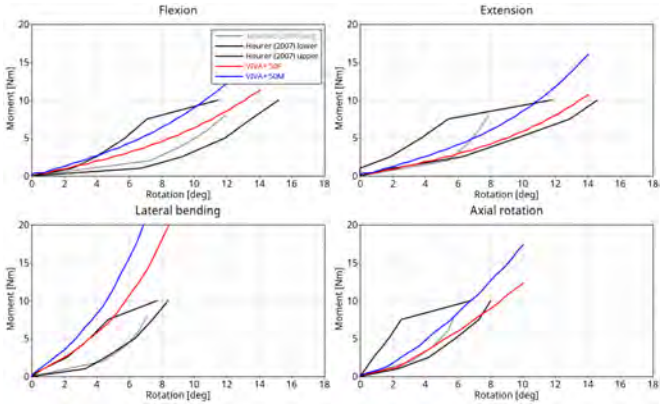

Fig. B 2. Step 2 – only disc.

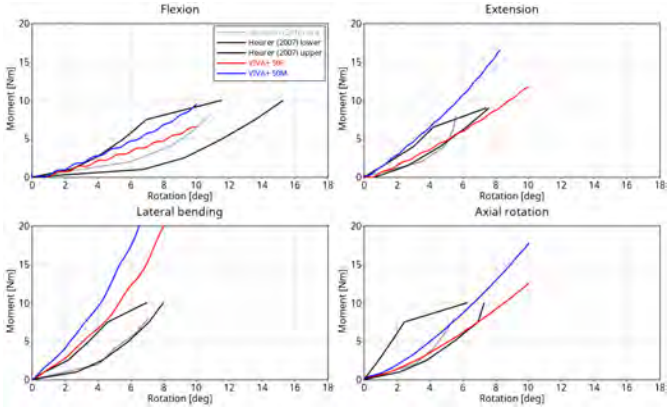

Fig. B 3. Step 3 – anterior longitudinal ligament added (ALL offset -1.5 mm).

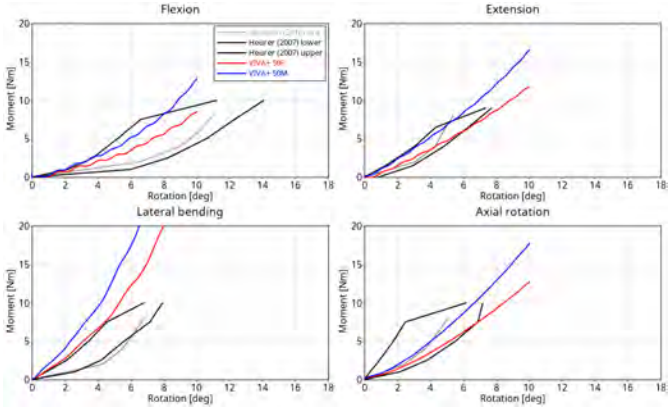

Fig. B 4. Step 4 – posterior longitudinal ligament added (PLL offset +1.5 mm).

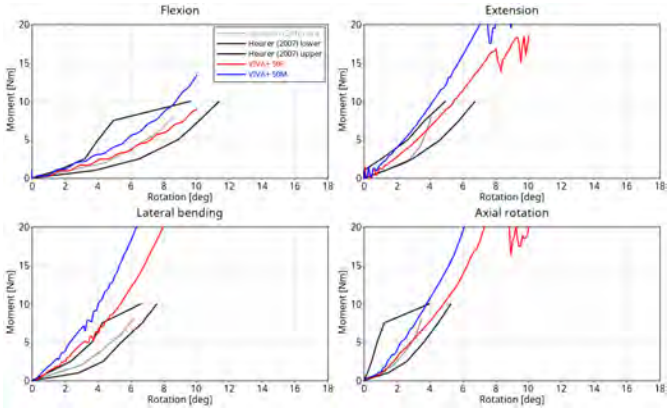

Fig. B 5. Step 5 - vertebrae arches added.

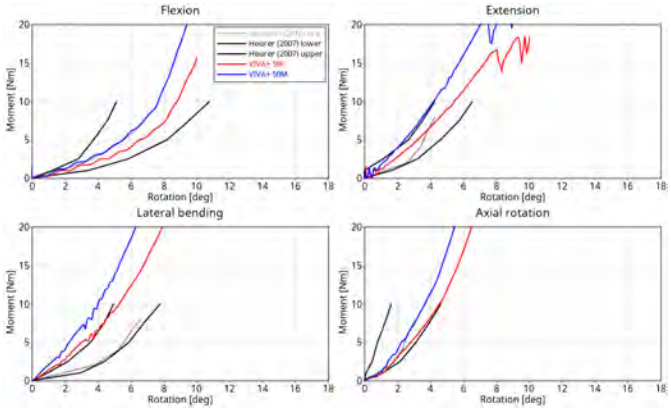

Fig. B 6. Step 6 – facet capsules ligaments added (FC offset +2 mm).

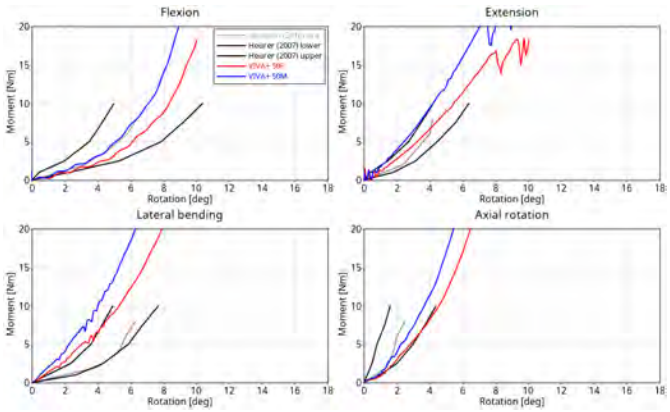

Fig. B 7. Step 7 – flavum ligaments added (FL offset +2 mm).

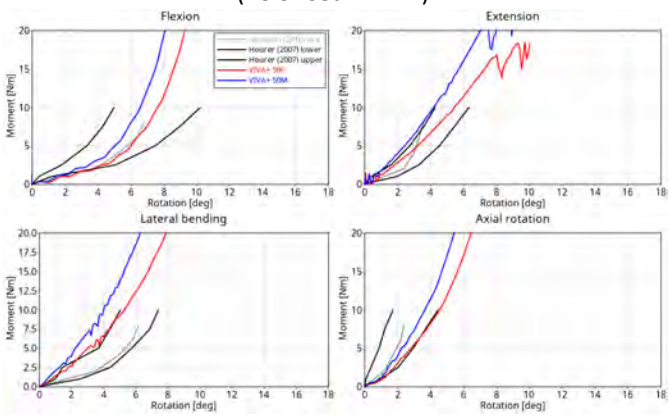

Fig. B 8. Step 8 – interspinous ligament added (ISL offset +5 mm).

X. APPENDIX C – VALIDATION OF SPINE ROTATIONAL KINEMATICS AND KINETICS

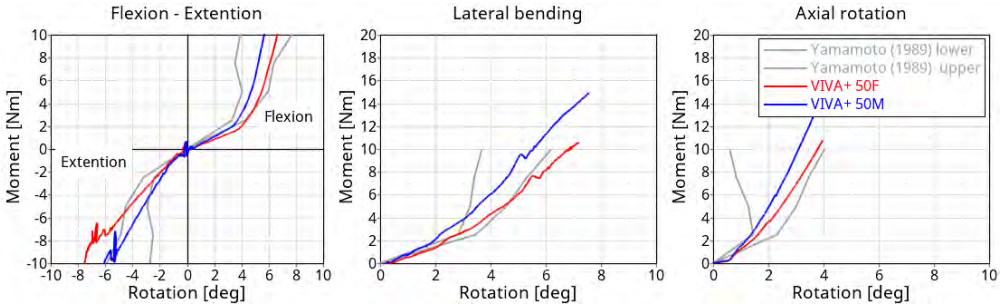

Fig. C 1. Validation of L1-L2 FSU rotational kinematics and kinetics [49], left: Flexion-Extension, mid: Lateral bending; and right: Axial rotation (same scale used in all plots for easier comparison of magnitudes)

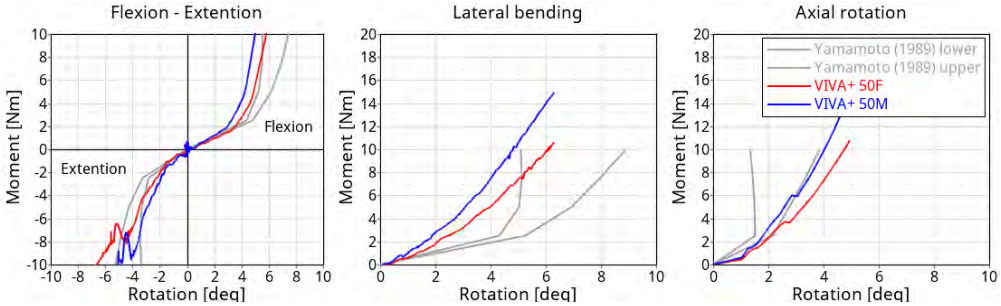

Fig. C 2. Validation of L2-L3 FSU rotational kinematics and kinetics [49], left: Flexion-Extension, mid: Lateral bending; and right: Axial rotation (same scale used in all plots for easier comparison of magnitudes)

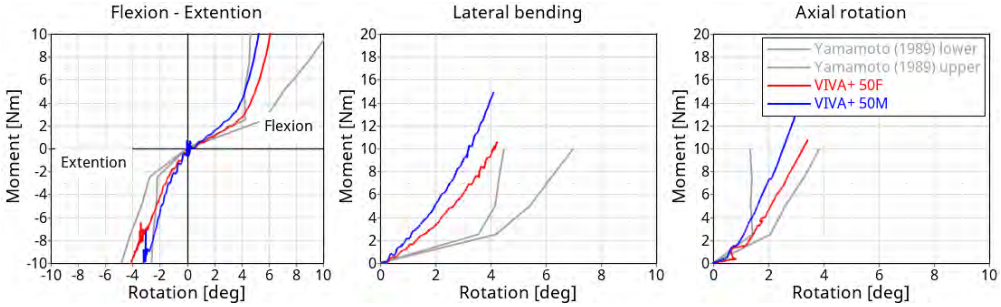

Fig. C 3. Validation of L3-L4 FSU rotational kinematics and kinetics [49], left: Flexion-Extension, mid: Lateral bending; and right: Axial rotation (same scale used in all plots for easier comparison of magnitudes)

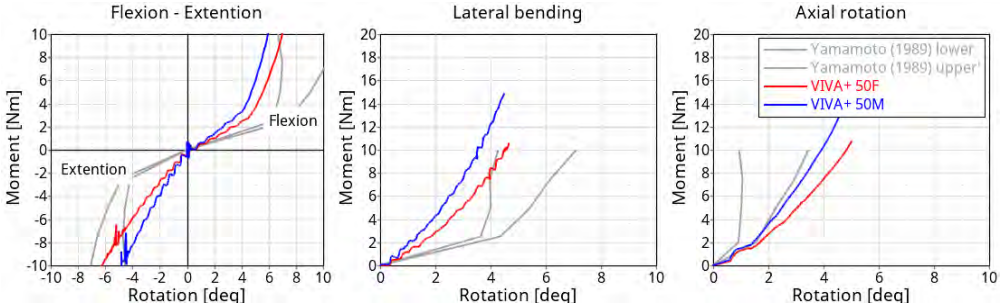

Fig. C 4. Validation of L4-L5 FSU rotational kinematics and kinetics [49], left: Flexion-Extension, mid: Lateral bending; and right: Axial rotation (same scale used in all plots for easier comparison of magnitudes)

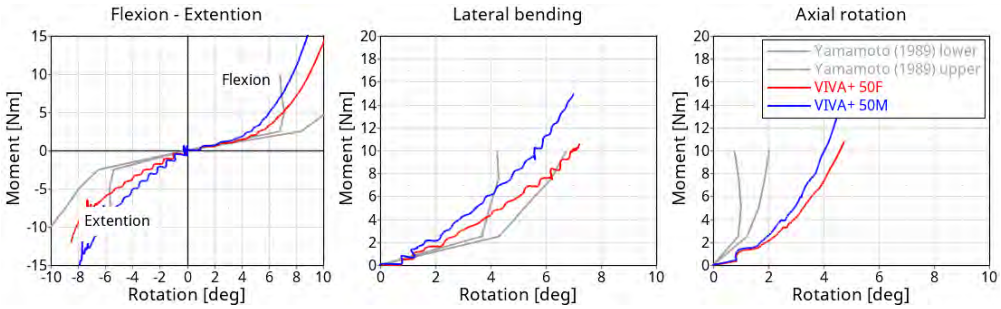

Fig. C 5. Validation of L5-S1 FSU rotational kinematics and kinetics [49], left: Flexion-Extension, mid: Lateral bending; and right: Axial rotation (same scale used in all plots for easier comparison of magnitudes)

XI. APPENDIX D – INCLUSION AND EXCLUSIONS OF PMHS TESTS

The following inclusion and exclusion criteria were deployed in this study.

- Data from tests on FSUs that were from embalmed subjects were excluded.
- Data from tests on FSUs from individuals with any history of spinal fractures/surgery or with osteoporosis were excluded.
- To enable a proper reproduction of the loading conditions that were present in the original tests, only data from tests on lumbar FSUs consisting of two or three vertebrae with discs were included in the development of the injury risk function.
- Data from tests on isolated vertebrae were excluded.
- Only data from tests where the inferior and superior ends of the FSUs were fixed to the loading device with some resins of known stiffness were included in the development of the injury risk function.
- Only test data from experiments on FSUs where the boundary conditions and initial spine curvatures were clearly defined were included.
- Only test data from experiments on FSUs where injury data, location of the injury and type of injury are available were included.
- Only tests that resulted in no injury or end-plate fracture were included.

XII. APPENDIX E – RECONSTRUCTION OF ORIGINAL TESTS

A. FSU in pure compression by Brinckmann *et al.* [53]

Brinckmann *et al*. carried out quasi-static compressive tests on 98 fresh spine FSUs from T12 to L5. These FSUs consisted of two adjacent vertebral bodies with intervertebral disc. The posterior elements were intact. The superior surfaces of the superior vertebrae and the inferior surfaces of the inferior vertebrae were attached to the loading devices using a block of high-density bone cement. In the tests, the caudal ends of the FSUs were rigidly fixated while the other ends were loaded at a rate of 1 kN/s. Prior to testing, the mid-plane of the disc was orientated parallel to the horizontal plane. Hence, there were no lordotic spine curvature present during spines testing. The tests were stopped at the first signs of fracture; load and fracture type were reported. An endplate fracture was reported in 41 of the 98 specimens tested.

The block of bone cement was modelled using *MAT_ELASTIC with Young's modulus 2.9 GPa and density 1.18 g/cm^3 in the LS-DYNA. The block was attached to the vertebrae using *CONSTRAINT_SHELL_IN_SOLID_PENALTY. Rigid shell surfaces were defined at the bottom and top surface of the modelled blocks to define boundary conditions. The bottom surface was constrained in all directions while loads were described for the upper surface using *LOAD_RIGID_BODY at 1 kN/s. Simulations were done for male and female separately and until the load reached 10 kN. LUMB_FLEX parameter was -1.0.

B. Lumbar FSU Pure compression by Duma *et al.* [56]

Duma *et al.* conducted compression tests on thawed FSUs from four male PMHSs. Each end of the FSUs was secured to the loading device using bonding compound. The mid-plane of the disc was positioned parallel with the potting cup, and the disc was centred in the potting cup. The specimens were loaded at a rate of 1 m/s until fracture. All the tests resulted in endplate fractures.

The bonding compound was modelled using the model *MAT_ELASTIC with Young's modulus 2.9 GPa and density 1.18 g/cm^3. The spine was connected to the models of the bonding compound using *CONSTRAINED_SHELL_IN_SOLID_PENALTY. The surfaces of the bottom and the top of the models of the bonding compound were lined with rigid shell elements to define boundary conditions. The bottom surface of the bottom model of the bonding compound was constrained in all directions. A prescribed load at 1 m/s was applied to the upper model of the bonding compound using *BOUNDARY_PRESCRIBED_MOTION. Individual simulations were carried out for each test condition. LUMB_FLEX parameter was -1.0.

C. Lumbar FSU Pure compression Granhed *et al.* [57]

Granhed *et al.* carried out quasi-static compression tests on 52 flexed lumbar FSUs. These units consisted of two adjacent vertebrae with intervertebral disc harvested from the fresh cadavers. The extremities of the specimens were attached to the loading devices using plastic cement. The posterior elements were intact. The specimens were initially flexed to 5°, 10° or 15° and thereafter loaded in axial compression at 12 mm/min. The tests were

stopped at fracture. Two types of fracture were reported; only the 29 segments that exhibited endplate fractures were reconstructed in this study. Five specimens that had no notable fracture after the tests were also reconstructed.

The plastic cement blocks were modelled using material model *MAT_ELASTIC with Young's modulus 0.75 GPa and density 1.44 g/cm^3. The blocks were attached to the vertebrae using *CONSTRAINT_SHELL_IN_SOLID_PENALTY. In addition, a surface of rigid shells was defined at the bottom and top surfaces of the two blocks. The FSU models were flexed to 5°, 10° and 15°, depending on load case to be modelled, in a pre-simulation by rotating both blocks. After the pre-simulation was carried out, the top block was constrained in rotation and the bottom block was constrained in all directions. Then the upper block was prescribed with a velocity of 12 mm/min to a displacement of about 4 mm using *BOUNDARY_PRESCRIBED_MOTION. A specific simulation was carried for each test configuration. LUMB_FLEX parameter was -1.0.

D. Lumbar FSU Flexion-compression by Hutton and Adams [54]

Hutton and Adams *et al.* tested 33 lumbar FSUs, some fresh, others thawed, with two vertebrae and an intervening disc. Both ends of the FSUs were attached to the loading devices using dental plaster. The specimens were initially flexed to a prescribed angle, followed by compressive loading at a rate of 3000 N/s. Loading was removed at the time of fracture. The loading produced endplate fractures in all the tests.

The dental plaster block was modelled using LS-DYNA material model *MAT_ELASTIC with Young's modulus 0.75 GPa and density 1.44 g/cm^3. The spine was connected to the blocks using the LS-DYNA keyword *CONSTRAINED_SHELL_IN_SOLID_PENALTY. Top and bottom surfaces of the two blocks were lined with rigid shell elements to define boundary conditions. The bottom surface of the bottom block was constrained in all directions. A pre-simulation was executed where the FSUs were flexed to the specified angle using *BOUNDRY_PRESCRIBED_MOTION of the upper block. After the pre-simulation was carried out, the top block was constrained in rotation while a compressive load that increased by 3 kN/s until the load reached ~15 kN was modelled using *BOUNDARY_PRESCRIBED_MOTION. Individual simulations were executed for each test condition. LUMB_FLEX parameter was -1.0.

E. Lumbar FSU Flexion-compression by Tushak *et al.* [55]

Tushak *et al.* applied flexion loading on 40 thawed lumbar FSUs following compression loading. These FSUs consisted of 3-vertebrae and intervening discs from fresh frozen PMHS. Both ends of the FSUs were potted/attached to the loading devices using a hardening resin. The superior loading device was constrained in translation in all directions but was allowed to rotate about the centre of the inferior potting cup (indicated with a cross in Fig. 4). The inferior loading devices was constrained in rotation but were allowed to translate in the X- and Z-direction. The lower potting was positioned parallel to the inferior endplate of the inferior vertebra and the upper potting was positioned parallel to superior endplate of the superior vertebra. In each of the tests a quasi-static compressive load was applied to the upper loading device until a block of honeycomb, placed underneath the bottom loading device, started to crush. Then a dynamic flexion load was applied, at a peak rate of 600 °/s, to the upper loading device. The tests produced endplate and cortical bone failures.

In the simulation of these tests, the resin block was modelled using model *MAT_ELASTIC with Young's modulus 2 GPa and density 1.5 g/cm^3. The vertebrae models were connected to the models of the resin blocks using the *CONSTRAINED_SHELL_IN_SOLID_PENALTY. The bottom and top surfaces of the blocks were lined with rigid shell elements to define boundary conditions. The inferior block was free to move in anterior-posterior and axial directions. The superior block was constrained in translation in all directions while allowed to rotate about the centre of the inferior potting cup. The lower block was modelled so that the inferior endplate of the lower vertebra was parallel to the bottom surface of the block. The first step in the simulations was to apply a quasi-static compressive load, a defined "crush force", that was maintained throughout the simulation. This "crush force" was attained by ramping up to the reported initial compressive load using a lead time selected based on iterations to avoid dynamic effects. A flexion was thereafter applied to the superior model of the resin block and its rate was based on the average rotational acceleration time plots provided in the publication (peak rate of 600 °/s). The termination time for the simulation was set based on the reported final flexion angle or flexion angle at fracture. Individual simulations were carried out for each test. LUMB_FLEX parameter was -1.0.

F. ***Data for the development of IRF***

Ref.	Sex	Age [years]	Level	Flexion [deg]	Falilure force [kN]	Reported CSA [mm^2]	Corr. CSA [mm^2]	Scaling factor
[53]	M	37	L12	0	7.80	1475	1111	1.06
[53]	F	79	L45	0	4.10	1665	1254	1.07
[53]	M	65	L12	0	4.60	1905	1435	1.20
[53]	M	70	L45	0	5.40	1825	1375	1.12
[53]	F	78	L23	0	3.30	1470	1107	1.01
[53]	M	49	L23	0	6.30	1385	1043	0.98
[53]	F	20	L45	0	6.30	1370	1032	0.97
[53]	F	57	L45	0	2.60	1305	983	0.94
[53]	M	63	L12	0	4.20	1360	1024	1.02
[53]	M	43	L23	0	8.80	1790	1348	1.11
[53]	M	22	L45	0	8.80	1435	1081	0.99
[53]	F	22	L34	0	6.20	1290	972	0.91
[53]	F	65	L12	0	2.70	1325	998	1.00
[53]	M	26	L12	0	4.30	1120	844	0.92
[53]	M	26	L34	0	4.80	1265	953	0.90
[53]	F	78	L12	0	3.10	1505	1134	1.07
[53]	M	65	L23	0	6.00	2165	1631	1.22
[53]	M	27	L23	0	8.20	1600	1205	1.05
[53]	M	27	L45	0	9.00	1780	1341	1.10
[53]	M	77	L45	0	5.30	1780	1341	1.10
[53]	F	31	L23	0	5.40	1290	972	0.94
[53]	F	31	L45	0	4.90	1300	979	0.94
[53]	F	20	L12	0	5.90	1165	878	0.94
[53]	F	20	L34	0	6.60	1425	1073	0.95
[53]	M	39	L12	0	8.20	1910	1439	1.20
[53]	M	39	L34	0	8.20	1950	1469	1.12
[53]	M	56	L12	0	2.90	1800	1356	1.17
[53]	M	56	L34	0	3.40	2525	1902	1.27
[53]	F	62	L23	0	3.20	1530	1152	1.03
[53]	F	43	L12	0	7.00	1030	776	0.88
[53]	F	43	L34	0	7.80	1270	957	0.90
[53]	F	47	L23	0	6.60	1775	1337	1.11
[53]	F	47	L45	0	7.90	2010	1514	1.17
[53]	M	69	L23	0	3.10	1775	1337	1.11
[53]	F	32	L23	0	7.50	1490	1122	1.01
[53]	M	53	L23	0	6.60	1540	1160	1.03
[53]	M	53	L45	0	7.90	1785	1345	1.10
[53]	M	45	L45	0	5.30	2190	1650	1.22
[53]	F	57	L12	0	2.70	1340	1009	1.01
[53]	F	57	L45	0	3.10	1860	1401	1.13
[53]	M	48	L23	0	5.70	1955	1473	1.16
[53]	M	48	L45	0	6.10	2270	1710	1.24

[54]	M	22	L34	7	10.78	1670	1294	1.08
[54]	M	31	L45	8	8.71	1980	1534	1.15
[54]	M	31	L12	4	11.57	1690	1309	1.14
[54]	M	31	L34	6	11.90	1800	1394	1.12
[54]	M	32	L23	6	6.86	1980	1534	1.15
[54]	M	33	L23	6	9.02	1780	1379	1.09
[54]	M	33	L45	8	10.78	1600	1239	1.03
[54]	M	46	L23	4	10.24	1730	1340	1.07
[54]	M	46	L45	6	11.24	2080	1611	1.18
[54]	M	46	L12	4	8.55	1440	1115	1.05
[54]	M	29	L34	10	5.15	1440	1115	1.00
[54]	M	38	L23	6	4.72	1290	999	0.93
[54]	M	38	L45	8	4.79	1390	1077	0.96
[54]	F	40	L34	8	6.11	1350	1046	0.97
[54]	F	47	L23	4	4.42	1350	1046	0.95
[54]	F	47	L45	6	4.55	1450	1123	0.98
[54]	F	50	L23	4	4.96	1800	1394	1.09
[54]	F	50	L12	6	3.85	1110	860	0.92
[54]	F	50	L34	7	4.70	1210	937	0.92
[54]	M	59	L23	5	8.86	2340	1813	1.25
[54]	M	59	L45	7	8.50	2500	1937	1.29
[54]	M	59	L23	6	7.11	2230	1727	1.22
[54]	M	59	L45	8	8.29	2000	1549	1.15
[54]	F	73	L23	4	3.70	1600	1239	1.03
[54]	F	73	L45	6	4.33	1590	1232	1.03
[55]	M	27	L3-L4-L5	23	4.67	1143	1344	1.10
[55]	M	66	L3-L4-L5	25	3.24	1345	1581	1.19
[55]	F	36	L3-L4-L5	19	2.44	907	1066	0.98
[55]	F	25	L3-L4-L5	17	4.38	685	805	0.85
[55]	M	47	L3-L4-L5	18	3.54	1035	1217	1.05
[55]	M	22	L3-L4-L5	23	5.06	1331	1565	1.19
[55]	F	46	L3-L4-L5	20	3.48	902	1061	0.98
[55]	F	51	L3-L4-L5	27	3.42	988	1162	1.02
[55]	F	71	L3-L4-L5	16	3.14	875	1029	0.96
[55]	F	56	L3-L4-L5	10	3.08	792	931	0.91
[55]	M	74	L3-L4-L5	15	4.80	1041	1224	1.05
[55]	M	49	L3-L4-L5	24	2.14	1062	1249	1.06
[55]	M	45	L3-L4-L5	24	3.16	1056	1242	1.06
[55]	M	63	L3-L4-L5	15	2.63	1045	1229	1.05
[55]	M	21	L3-L4-L5	23	3.14	1598	1879	1.30
[55]	M	27	T12-L1-L2	13	3.42	1049	1233	1.15
[55]	M	66	T12-L1-L2	9	3.09	1271	1494	1.27
[55]	F	36	T12-L1-L2	4	2.45	781	918	0.99
[55]	F	25	T12-L1-L2	22	3.14	676	795	0.93
[55]	M	47	T12-L1-L2	14	2.96	1035	1217	1.15
[55]	M	22	T12-L1-L2	15	3.48	994	1169	1.12
[55]	F	56	T12-L1-L2	8	3.13	738	868	0.97
[55]	M	74	T12-L1-L2	11	2.78	912	1072	1.07
[55]	M	49	T12-L1-L2	15	4.31	883	1038	1.06
[55]	M	21	T12-L1-L2	24	4.21	1205	1417	1.24

[56]	M	45	L23	0	12.78	NA	NA	1.11
[56]	M	45	L45	0	13.07	NA	NA	1.11
[56]	M	45	L12	0	11.20	NA	NA	1.11
[56]	M	45	L34	0	12.60	NA	NA	1.11
[57]	F	74	L12	0	2.93	NA	NA	1.00
[57]	F	74	L34	0	4.23	NA	NA	1.00
[57]	F	69	L23	0	3.58	NA	NA	1.00
[57]	F	69	L34	0	4.17	NA	NA	1.00
[57]	F	69	L23	0	1.63	NA	NA	1.00
[57]	F	69	L45	0	3.26	NA	NA	1.00
[57]	M	18	L23	0	7.65	NA	NA	1.11
[57]	M	24	L45	0	9.12	NA	NA	1.11
[57]	M	34	L23	0	6.02	NA	NA	1.11
[57]	M	34	L45	0	6.18	NA	NA	1.11
[57]	F	35	L23	0	5.21	NA	NA	1.00
[57]	F	35	L45	0	5.29	NA	NA	1.00
[57]	M	20	L34	0	10.09	NA	NA	1.11
[57]	M	71	L23	0	4.31	NA	NA	1.11
[57]	M	71	L45	0	4.56	NA	NA	1.11
[57]	M	75	L23	5	5.70	NA	NA	1.11
[57]	M	75	L45	5	5.21	NA	NA	1.11
[57]	F	78	L12	5	1.63	NA	NA	1.00
[57]	F	78	L34	5	1.62	NA	NA	1.00
[57]	M	34	L23	5	5.86	NA	NA	1.11
[57]	M	34	L45	5	8.74	NA	NA	1.11
[57]	M	41	L23	5	6.68	NA	NA	1.11
[57]	M	41	L45	5	8.55	NA	NA	1.11
[57]	M	17	L45	5	5.05	NA	NA	1.11
[57]	M	26	L23	5	6.51	NA	NA	1.11
[57]	M	26	L34	5	9.56	NA	NA	1.11
[57]	M	20	L12	10	8.30	NA	NA	1.11
[57]	M	33	L23	10	7.81	NA	NA	1.11